SIMULATION OF SPACECRAFT POWER SYSTEMS USING A MODULAR STATE VARIABLE APPROACH

by

Robert Mark Nelms

Dissertation submitted to the Faculty of the
Virginia Polytechnic Institute and State University
in partial fulfillment of the requirements for the degree of

DOCTOR OF PHILOSOPHY

in

Electrical Engineering

APPROVED:

L.L. Grigsby, Co-chairman

A.G. Phadke, Co-chairman

S. Rahman

C.E. Nunnally

H.D. Sherali

June, 1987

Blacksburg, Virginia

SIMULATION OF SPACECRAFT POWER SYSTEMS USING A MODULAR STATE VARIABLE APPROACH

by

Robert Mark Nelms

Co-Chairmen: L.L. Grigsby and A.G. Phadke
Electrical Engineering

(ABSTRACT)

The power requirements for future spacecraft power systems will be on the order of a few hundred kilowatts to a few megawatts. Because of these power levels, a high-voltage, high-power distribution subsystem may be utilized to transmit power from the source to the different loads. Using current state-of-the-art power conditioning electronics, complex series and parallel configurations will be required at the interface between the source and the distribution subsystem and between the distribution subsystem and the loads.

The dynamic response of such a spacecraft power system may be obtained using a general purpose program such as SPICE2. However, for large and complex spacecraft power systems, the input file will be large and complex with correspondingly large computation times. As an alternative, the spacecraft power system can be considered as an interconnection of modular components. Each component is treated as a two-port network, and a state model is written with the port voltages as the inputs. The state model of each component is solved using the state transition matrix and assuming that the port voltages are clamped for each time step. This calculation proceeds as if all

two-port networks are decoupled. After the state variables have been updated, the inputs to all components are calculated using network analysis principles. The solution procedure alternates between solving the dynamic model of all components and the network equations for the component inputs.

The modular state variable approach and SPICE2 are compared using two example systems. This comparison shows the advantages of the modular state variable approach. First, for the modular state variable approach the system is considered as an interconnection of modular components. In SPICE2, the system is treated as an interconnection of circuit elements. As a result, the system description for large and complex spacecraft power systems is much larger and more complex than a modular state variable description. Secondly, the modular state variable approach requires less CPU time than SPICE2. For one of the example systems presented here, the modular state variable approach uses one-twentieth of the CPU time used by SPICE2.

ACKNOWLEDGEMENTS

My doctoral program has been unusual in the fact that I have carried out research for my dissertation at Auburn University while remaining enrolled at Virginia Polytechnic Institute. Therefore, I wish to express my sincerest appreciation to people at Auburn University and Virginia Polytechnic Institute.

I would like to thank my advisor Dr. L.L. Grigsby for his guidance and support which has made graduate study an enjoyable experience. I would also like to thank the other members of my committee: Dr. A.G. Phadke, who has served as co-advisor, Dr. S. Rahman, Dr. C.E. Nunnally, and Dr. H.D. Sherali.

Completion of degree requirements would not have been possible without the help of The author also wishes to acknowledge the financial support of the Energy Research Group while attending Virginia Polytechnic Institute.

The work reported in this dissertation was supported by the Space Power Institute at Auburn University and the SDIO Innovative Science and Technology Office and the Defense Nuclear Agency under DNA contract DNA 001-85-C-0183.

I would also like to express my gratitude to for skillful typing of this document.

Finally, and most importantly, I want to thank my family for their patience and support during this endeavor.

Table of Contents

LIST OF FIGURES

LIST OF TABLES

CHAPTER 1. INTRODUCTION

The electrical power requirements for spacecraft of the future will be on the order of a few hundred kilowatts to a few megawatts [1,2]. These power levels, which are one to two orders of magnitude greater than current power requirements, dictate utilizing a high-voltage, high-power (HVHP) distribution subsystem to transmit power from the source to the different user loads. Because of these power levels, this distribution subsystem must operate at voltages higher than the 28 volts commonly used today. At this point, NASA has considered distribution voltages up to 440 volts [3]. Future multi-megawatt systems will probably necessitate using even higher distribution voltages.

The HVHP distribution subsystem may be either ac or dc. One advantage of dc over ac is that of familiarity, since the distribution subsystem of most all spacecraft has been dc. An ac distribution subsystem offers the traditional advantages of ac over dc: the ability to change voltage levels easily with transformers and the natural zero crossings of the currents, which are an aid in clearing faults. NASA is investigating three alternatives for the space station: high voltage dc (150 V - 270 V), 400 Hz ac and 20 kHz ac [3]. High voltage dc has been proposed because of the experience gained with previous spacecraft power systems. 400 Hz ac has been utilized on aircraft, so experience with this technology exists.

However, potential concerns are acoustic noise and electromagnetic interference [3,15]. The newest technology, which has never been employed, is the 20 kHz ac system. It is attractive because components are small and lightweight at this high frequency [3]. Even though NASA is considering only these three alternatives for the space station, other frequencies may be selected for other applications.

In spacecraft power systems, different voltage and current levels must be available for the different user loads. Some of these loads may require ac, while others may need dc. In addition, the source for the spacecraft power may generate power at low voltage and high current which must be converted to high voltage and low current for transmission to the different loads. The source power may be converted from dc to ac or ac to dc depending on the source type and HVHP distribution subsystem. As a result, electronic power conversion equipment is an integral part of the spacecraft power system.

Using current state-of-the-art power conditioning electronics, complex series and parallel configurations are required to perform the necessary conversions at the interface between the source and the distribution subsystem and between the distribution subsystem and the loads. The output of many dc-dc converters may be connected in series in order to achieve a desired distribution voltage. Parallel connection of conversion equipment will be necessary because currents in the system could be on the order of thousands of amperes [2]. Even

if the technology existed to handle these current levels, parallel connections would be desirable from a reliability standpoint.

In the design of spacecraft power systems, many factors such as weight, volume, efficiency and voltage regulation must be considered. In addition, the dynamic response of different designs must be evaluated. System transients will result from events such as load changes. For example, scientific experiments on the space station will be switched on and off. The effects of these switchings events must be investigated to determine if they might in some way be detrimental to secure operation of the spacecraft power system.

The dynamic response of a spacecraft power system may be studied using a general purpose program such as SPICE2 [4]. However, for large and complex spacecraft power systems, the input file will be large and complex with correspondingly large computation times. This large and complex input file results from representing the spacecraft power system as an interconnecton of circuit elements, i.e. resistors, capacitors, transistors, etc. A more suitable representation is to consider the spacecraft power system as an interconnection of modular components. The need for a modular approach has also been recognized by Cho and Lee [5]. Each modular component is treated as a two-port network, and a mathematical model is written. For this research, state variable techniques have been utilized to write a state model for each component. The state variables are selected to be the voltage for any capacitors and the current for any inductors contained

in the component. The inputs for the state model are the port voltages. This technique is illustrated in Chapter's 2 and 3.

In [5], the computer program EASY5 by Boeing Computer Services was used to combine all component models into an overall system model which is then solved. A different approach is taken in this work. The state model for each component is solved using its state transistion matrix. For this computation, the port voltages are clamped. The calculation of the new values for the state variables proceeds as if all two-port networks are decoupled. After the state variables for each component have been updated, the inputs are then calculated using network analysis principles. In this calculation, all two-port networks are interconnected. This alternating solution technique is very similar to that employed in transient stability studies of utility power systems [6]. Chapter 4 presents the details of the solution procedure.

Chapter 5 presents results from the simulation of example systems. In the first system, a parallel-loaded resonant converter is connected to a transmission line which supplies a bridge rectifier with a resistive load. The second system consists of two boost dc-dc converters connected in series supplying a resistive load. These examples show that the modular state variable approach is much faster computationally than SPICE2. The ratio of the CPU time for SPICE2 to the CPU time for the modular state variable approach is approximately 6 for the first example and 20 for the second example. This savings

in CPU time can be attributed to modular component modeling and to component level simulation. A third example examines the effects of varying the time step in the solution algorithm.

CHAPTER 2. MODELING OF DC-DC CONVERTERS

2.1 Introduction

If the source for the spacecraft power system generates a dc voltage and a dc distribution subsystem is employed, dc-dc converters will be utilized at the interface between the source and the distribution subsystem. Because of the projected power levels, the distribution subsystem may operate at a higher voltage than the source. Therefore dc-dc converters will be needed to step up the source voltage. DC-DC converters will also be used to change the distribution subsystem voltage to levels compatible with the various loads. This chapter describes the basic operation of dc-dc converters. It also presents a dc-dc converter model for the simulation of spacecraft power systems.

2.2 DC-DC Converters

In ac systems, transformers are used to change the voltage level. DC-DC converters can be utilized to change the voltage level in a dc system. Three basic converter topologies are shown in Figure 2.1. The basic elements of these topologies are a transistor, diode, and inductor. A capacitor is utilized for filtering the output voltage. Although a bipolar transistor is used in each topology, a field-effect transistor, thyristor, or other device may be utilized. The bipolar transistor is operated as a switch by applying a pulse voltage to the

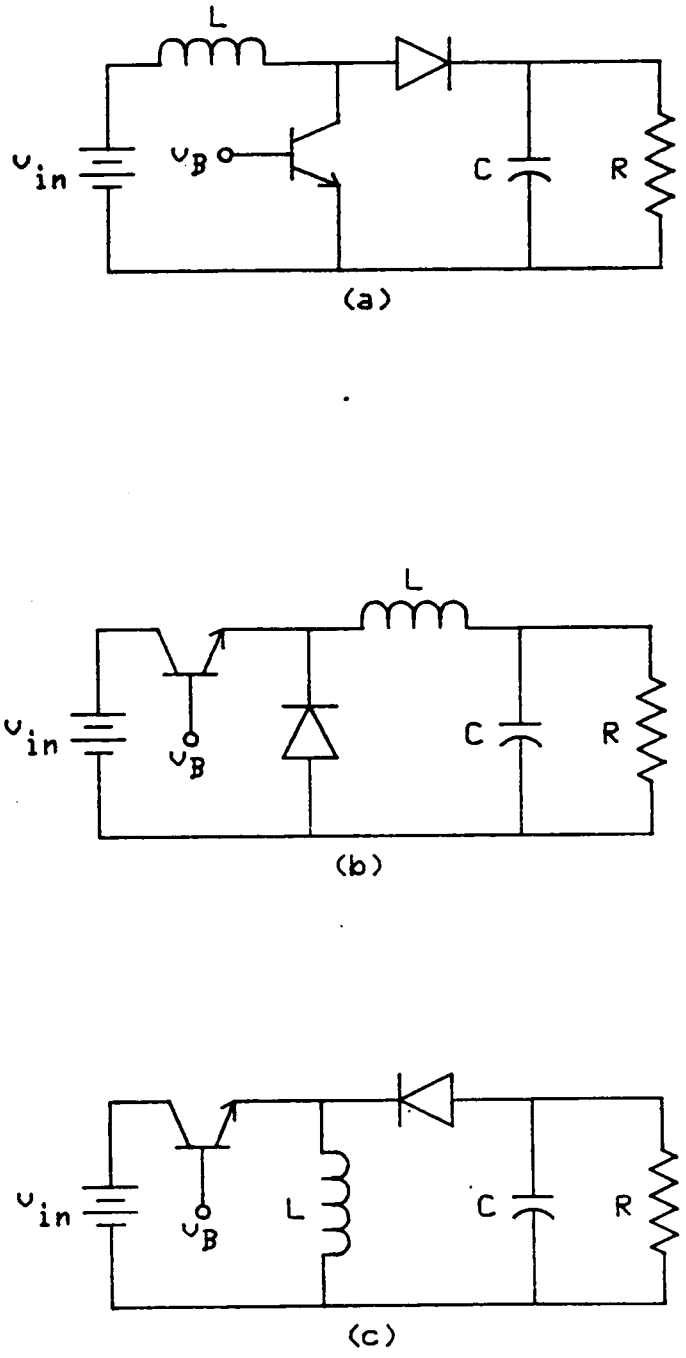

Figure 2.1. Basic dc-dc converter topologies: (a) boost, (b) buck, (c) buck-boost.

base. The amplitude of this pulse is large enough to drive the transistor into saturation. Application of this pulse voltage causes the transistor to alternate between saturation and cutoff. As a result, the dc-dc converter is very efficient, because the power dissipated in the transistor is small when it is in saturation or cutoff. The efficiency is slightly reduced by switching losses which occur with the transition from saturation to cutoff and vice versa. The switching losses may be reduced by adding a snubber circuit in parallel with the transistor.

Figure 2.2 shows the voltage waveform applied to the base of the transistor. In this waveform, the transistor on-time is given by DT_S where D is the duty ratio and T_S is the switching period, which is the reciprocal of the switching frequency f_s. The output voltage of the dc-dc converter may be controlled using either pulse-width modulation, frequency modulation or a combination of the two [7]. T_S is held constant and the on-time of the transistor is varied in pulse-width modulation. For frequency modulation, the on-time of the transistor is held constant and T_S is varied.

One cycle of converter operation may be divided into three intervals. In the first interval, the transistor conducts and the diode blocks. The second interval is characterized by the transistor blocking and the diode conducting. If one cycle of operation is divided between these two intervals, the converter is operating in the continuous mode. A third interval may exist if the load or switching

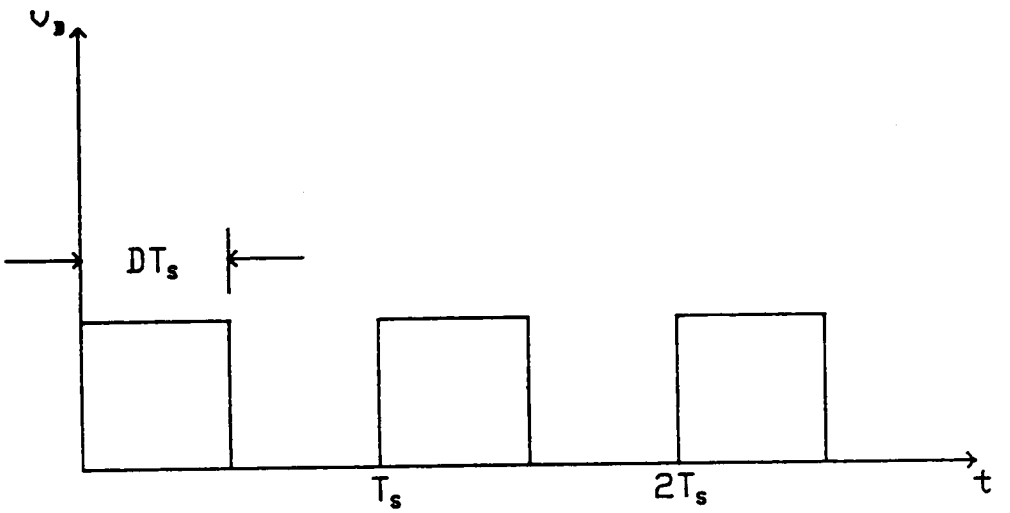

Figure 2.2. Transistor base voltage waveform.

frequency are adjusted so that the inductor current reaches zero before the end of the cycle. In this interval both the transistor and diode are blocking. The existence of this interval indicates that the converter is operating in the discontinuous mode.

The first topology shown in Figure 2.1 is the boost converter. The ideal voltage gain for this topology is 1/(1-D). Since D is always less than one, the output voltage will always be greater than the input voltage. Theoretically, this gain could be infinity. However, nonidealities in the circuit such as the resistance of the inductor limit the gain [8]. The buck converter, also shown in Figure 2.1, has an ideal gain of D, so the output voltage is always less than the input voltage. The third topology in Figure 2.1 is the buck-boost converter which has an ideal gain of D/(1-D). Depending on the value of D, this topology may buck or boost the input voltage. The output voltage is inverted for this topology. The ideal gains given here may be derived using the principle of constant flux linkages [8].

2.3 State Model for a DC-DC Converter

The modeling and analysis of DC-DC converters has been and continues to be a heavily researched area. The IEEE Power Electronics Specialists Conference Records contain many papers on this area of research. TESLAco has published three books which contain a collection of papers on this subject [8-10]. A bibliography of papers on this subject can be found in [11]. Papers may also be found in

publications such as the IEEE Industry Applications Society Transactions or the Proceedings of the Intersociety Energy Conversion Engineering Conference. Books have also been written which deal with this subject [11-13,32].

Cuk and Middlebrook have analyzed dc-dc converters using state-space averaging [33,34]. For this technique, the transistor and diode are modeled by ideal switches. Since one cycle of converter operation may be divided into three intervals, three linear networks describe converter operation. State equations are written for each linear network using the capacitor voltage and inductor current as the state variables. The sets of state equations are then averaged together to form a state model which approximately describes converter operation.

For example, in the continuous conduction mode, the converter is represented by two sets of state equations. Let the state equations for the interval $[0, DT_S]$ be

$$\dot{\underline{x}} = A_1\underline{x} + B_1\underline{u} \tag{2.1}$$

and the state equations for the interval $[DT_S, T_S]$ be

$$\dot{\underline{x}} = A_2\underline{x} + B_2\underline{u} \tag{2.2}$$

where $\underline{x}$ and $\underline{u}$ are the state vector and input vector, respectively. These equations are averaged in the following manner

$$\dot{\underline{x}} = D(A_1\underline{x} + B_1\underline{u}) + D'(A_2\underline{x} + B_2\underline{u}) \tag{2.3}$$

In this equation, $D' = (1-D)$. Rearranging (2.3) yields

$$\dot{\underline{x}} = (DA_1 + D'A_2)\underline{x} + (DB_1 + D'B_2)\underline{u} \tag{2.4}$$

which is a linear continuous system.

Equation (2.4) is the basic state-space averaged model. Beginning with this equation, a canonical circuit model can be developed for dc-dc converters operating in the continuous mode. A canonical circuit model can also be derived for a dc-dc converter operating in the discontinuous mode. Three sets of state equations are averaged for this mode of operation. The fundamental approximation in this modeling approach is that the matrix e^{At} can be approximated by the first two terms in its power series representation, $I + At$ [33]. This is equivalent to requiring low output voltage ripple [33].

In [33] and [34], the transistor and diode are modeled by ideal switches. Averaging techniques have also been applied when different models are employed for these devices. Polivka, Chetty, and Middlebrook [35] included a small resistance for each device when they are conducting. For the continuous mode, two sets of state equations are written. One set of equations contains the resistance of the transistor, and the other set contains the diode resistance. One linear continuous system of equations is obtained through state-space

averaging. Alternatively, the transistor and diode may be represented by a voltage source in series with a small resistance [36]. Instead of averaging the state equations, the circuit components may be averaged to produce approximate continuous circuit models [37].

When the fundamental approximation of the state-space averaging technique cannot be made, discrete modeling techniques may be employed. Models of dc-dc converters for computer simulation may be developed using these techniques [29,38,39,43-45]. The state transistion matrix is used to solve the state equations in all but [44]. State-plane anlaysis is utilized in [44] to predict transient behavior of a dc-dc converter. Discrete modeling and state-space averaging are compared in [40]. Shortt and Lee employed both discrete and averaging techniques to develop an improved circuit model for dc-dc converters [41,42].

The list of references on the modeling and analysis of dc-dc converters given here is not all-inclusive. However, it presents many of the analytical techniques employed in the study and design of dc-dc converters. Many of these techniques are compared in [46] and [47].

All of these papers have examined single converter systems. The large and complex spacecraft power systems of the future will contain series and parallel configurations of dc-dc converters. In order to simulate such a system, a modular converter model must be developed. Cho and Lee were the first to recognize this [5]. The dc-dc converter is treated as a two-port network, and a mathematical model is written

in terms of the port quantities. In this work, a state model is written with the port voltages as the inputs. The state variables are the voltge for any capacitors and current for any inductors contained in the converter.

In writing the mathematical model for the two-port representation of the dc-dc converter, a model for the transistor and diode must be selected. In most analyses, the transistor and diode are modeled by ideal switches. The switching device is a short circuit when conducting and an open circuit when blocking. Using this representation, converter operation can be described by three state models. Each state model corresponds to a linear network which exists for each interval of converter operation. In [35] and [36], the transistor and diode are modeled by either a small resistance or a small resistance and voltage source when they are conducting. They are modeled as open circuits when blocking. Three linear networks and state models result from this transistor and diode representation. However, if the transistor and diode are modeled by piecewise linear resistors, one piecewise linear network and one state model can be used to describe converter operation. Each interval of operation can be simulated by using the appropriate resistance values for the transistor and diode. When a device is conducting, it is modeled by a small resistance, and when it is blocking, a large value of resistance is employed. The value used is calculated from the manufacturer's data sheet for the particular device. The "on" resistance is the

value used when the device is conducting and is calculated by dividing the forward voltage drop by the rated current. When the device is blocking, the "off" resistance is employed and calculated from the maximum reverse current at a specified voltage. In addition, modeling the transistor and diode by piecewise linear resistors accounts for conduction losses which are neglected if switching devices are treated as ideal switches.

The state model for a boost converter is developed as an example. The network for formulating the state model is given in Figure 2.3. The transistor is represented by resistance R_T and the diode by resistance R_D. R_C is the effective series resistance of the capacitor, and R_L is the series resistance of the inductor. The state variables are the capacitor voltage and inductor current, and the inputs are port voltages. The technique used to develop the state model can be found in [14]. The state model is given on the next page.

$$\frac{d}{dt}\begin{bmatrix} i_L \\ v_C \end{bmatrix} = \begin{bmatrix} -\left\{\dfrac{R_L + \dfrac{R_T R_D}{R_T + R_D}}{L}\right\} & 0 \\ 0 & \dfrac{-1}{R_C C} \end{bmatrix} \begin{bmatrix} i_L \\ v_C \end{bmatrix}$$

$$+ \begin{bmatrix} \dfrac{1}{L} & \dfrac{-R_T}{(R_T + R_D)L} \\ 0 & \dfrac{1}{R_C C} \end{bmatrix} \begin{bmatrix} v_1 \\ v_2 \end{bmatrix} \qquad (2.5)$$

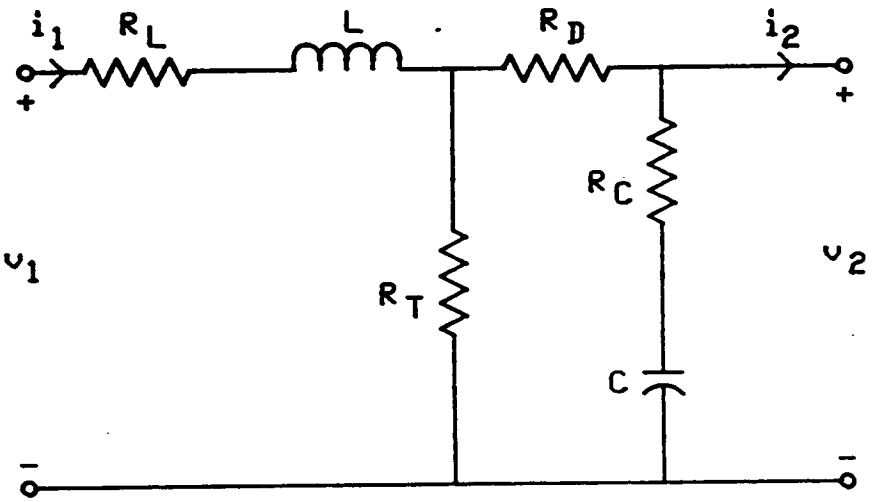

Figure 2.3. Network for formulating boost converter state model.

CHAPTER 3. MODELING OF SERIES RESONANT CONVERTERS

3.1 Introduction

As an alternative to a dc distribution subsystem, the source power may be transmitted to the loads over an ac distribution subsystem. The natural zero crossings of the currents and the capability of changing voltage levels easily with transformers makes ac transmission attractive. However, weight and volume constraints necessitate using a frequency higher than 60 Hz. NASA is currently considering two frequencies, 400 Hz and 20 kHz [3]. 400 Hz has been used extensively in aircraft, while 20 kHz is a new technology. The advantage of 20 kHz over 400 Hz is that the weight and volume of components is reduced. Even though NASA is only considering these two frequencies for the Space Station, other frequencies may be selected for future spacecraft power systems.

If the source for the spacecraft power system operates at a dc voltage, power conditioning equipment is needed for the conversion from dc to ac. The 20 kHz power system proposed by NASA will use resonant converters for this conversion [15]. This chapter describes the operation of two types of resonant converters and presents the development of a two-port state model for one of these.

3.2 Series Resonant Converters

Figure 3.1 shows two types of series resonant converters. The first is the series-loaded resonant converter or Schwarz inverter which was developed by Francis C. Schwarz [16,17]. In this converter, the load R is connected in series with an LC circuit. The second is the parallel-loaded resonant converter or Mapham inverter which was developed by Neville Mapham [18]. The load R is connected in parallel with the capacitor in the LC circuit.

The series-loaded resonant converter has a current source type output because the load is connected in series with the inductor. This converter is intolerant of large values of R; however, it will continue to operate even if R equals zero. In comparison, the parallel-loaded resonant converter has a voltage source type output because the load is connected in parallel with the capacitor. This configuration is intolerant of small values of R. In fact, extremely small values cause the output voltage to decrease almost to zero. In other words, this converter shuts itself down. Engineers interested in the design and operation of 20 kHz power systems debate whether the series-loaded or parallel-load resonant converter should be used based on how the two converters react to faults. The parallel-loaded converter will protect itself by shuttng down. In contrast, the series-loaded resonant converter will continue to feed current to the fault giving the protection system an opportunity to clear the fault.

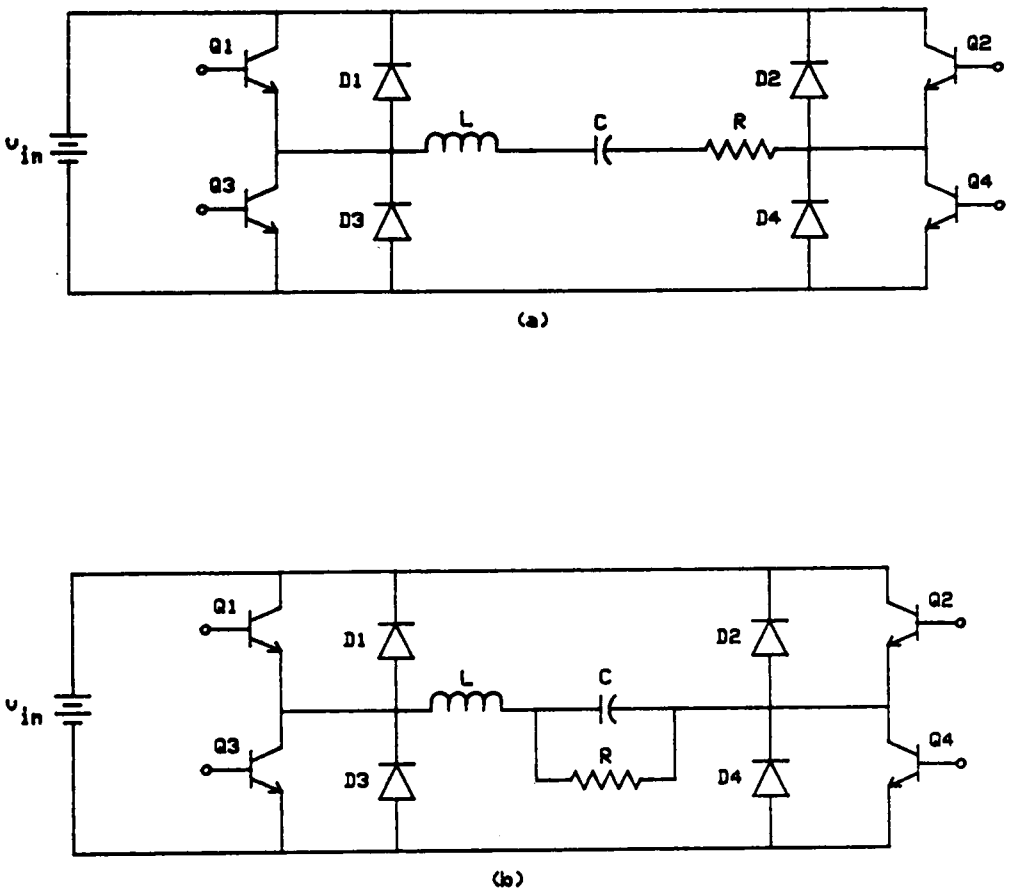

Figure 3.1. Resonant converter topologies: (a) series-loaded, (b) parallel-loaded.

The operation of the resonant converter will be described using Figure 3.1. Only the continuous mode of operation will be considered in this discussion. Full-bridge configurations are shown in this figure. Half-bridge configurations, which perform the same operation, may be found in the literature [18-20]. A pulse of sufficient amplitude to saturate the transistors is applied to the base of each transistor. The voltage applied to the base of the transistors is shown in Figure 3.2. This pulse has a fixed duty ratio of 0.5, so a transistor is saturated half of the time and is in cut-off the other half of the time. Control of the output quantity is achieved through frequency modulation (i.e. varying T_S). The frequency of the output quantity is the switching frequency f_S.

The transistors in Figure 3.1 are switched on in pairs. Q1 and Q4 conduct together while Q2 and Q3 are turned off. When Q2 and Q3 are switched on, Q1 and Q4 are turned off. Switching the transistors in this manner alternately applies a voltage of $+ v_{in}$ and $- v_{in}$ to an LC circuit. The conversion from a dc voltage to an ac voltage is achieved through this switching action and the LC circuit.

Diodes D1-D4 conduct depending on the relationship between the switching frequency f_S and the resonant frequency of the LC circuit $f_0 = 1/2\pi\sqrt{LC}$. If $f_S < f_0$, then $T_S > T_0$, which is the reciprocal of f_0. The inductor current goes through zero before tansistors Q1 and Q4 are turned off. Since current does not flow very readily from emitter to collector in a bipolar transistor, an alternate path must be given for the current. This alternate conduction path is provided

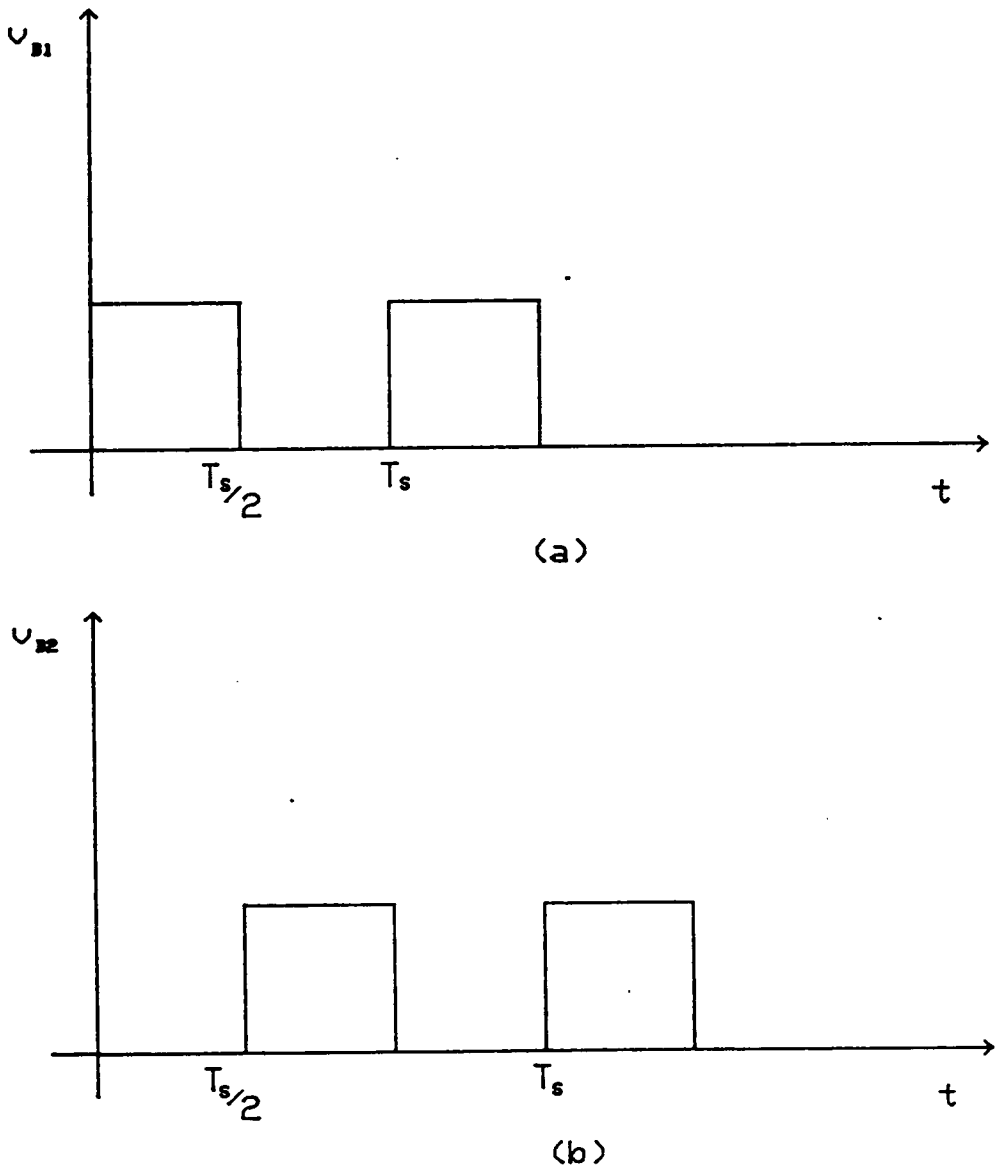

Figure 3.2. Voltage applied to base of transistors (a) Q1 and Q4, (b) Q2 and Q3.

by diodes D1 and D4. They conduct until Q2 and Q3 are turned on. Q2 and Q3 conduct until the inductor current goes positive at which time D2 and D3 conduct until Q1 and Q4 are turned on. If, on the other hand, $f_S > f_0$, then $T_S < T_0$. Before the inductor current reaches zero, Q1 and Q4 are switched off. Therefore, the current is transferred to D2 and D3 until the inductor current reaches zero. Then Q2 and Q3 conduct. These transistors conduct until they are turned off and Q1 and Q4 turned on. However, since the current through Q2 and Q3 has not yet reached zero, current is transferred to D1 and D4. The conduction paths provided by the diodes return any excess energy in the LC circuit to the source thus preventing voltage instability [17].

Although bipolar transistors are employed as the switching devices in Figure 3.1, thyristors may be utilized. If thyristors are used as the switching devices, the resonant converter is controlled such that $f_S < f_0$. The thyristors are naturally commutated because the current flowing through the thyristor goes to zero due to the action of the LC circuit. f_S can be adjusted so that a pair of thyristors can recover their blocking characteristics before the other pair of thyristors is triggered. Operation of the converter such that $f_S > f_0$ will require forced commutation of the thyristors, which will require additional circuitry.

Most resonant converters are operated in the frequency range $f_0/2 < f_S < f_0$. Operation in this range produces very low stress on

the transistors or thyristors and low switching losses because the current flow through these devices reaches zero before the device must be turned off. This is one of the advantages in using resonant converters. A second advantage is that the resonant converter generates output quantities which are almost purely sinusoidal. The output quantities contain a dominant fundamental component at a frequency of f_s and the odd harmonics of the switching frequency. The relationship between f_s and f_0 determines the magnitude of these additional harmonic components. As f_s approaches f_0, the magnitude of these components decrease. Square wave inverters require an output filter to produce an almost sinusoidal output. However, in the resonant converter, the filtering is an integral part of the power conversion process. Because the resonant converter generates an almost sinusoidal output, it produces little electromagnetic interference. Another very important point is that resonant converters may be parallelled quite easily [15]. Thus, as the system load increases, more resonant converters may be connected in parallel to supply the new load level.

Series resonant converters have two disadvantages. The first is that of complexity. A half-bridge configuration requires two transistors, and a full-bridge configuration reqiures four. A control circuit is needed for each transistor. For the full-bridge configuration, the transistors are switched in pairs. Therefore, the control circuits for these transistors must be synchronized. The

second disadvantage is the high currents which flow through the switching devices because of the resonant circuit.

3.3 State Model for the Series Resonant Converter

Much of the previous research into the modeling and analysis of series resonant converters has examined their use for dc-dc conversion. In this case, the load on the converter is a rectifier which is usually connected to the converter through a transformer. Researchers have investigated the steady-state operation and control of this configuration [16,17,19,21-25]. Some of these analyses have examined operation of the converter in terms of the conduction time of one of the diodes [17,21,22]. Vorperian and Cuk [19] analyzed the resonant converter in terms of the ratio f_s/f_0 and the load R. In addition, they have studied the effects of small pertrubations in f_s and the input voltage on converter operation [20]. The resonant converter has also been analyzed using state-plane analysis [26,27]. King and Stuart simulated the series resonant converter using a nonlinear discrete time model [28]. They have also proposed a new control method to prevent converter overload and examined the interaction of the resonant converter with the transformer [48,49].

All of the anlayses given in the previous paragraph deal with utilization of the series resonant converter for dc-dc conversion. For spacecraft power systems, the resonant converter will be used for the conversion from dc to ac. The power generated by a dc source will

be converted to ac for transmission to the loads. Mapham [18] investigated using the parallel-loaded resonant converter to produce an ac voltage from a dc source. The spacecraft power systems of the future, however, will require many resonant converters. Therefore, a modular state model must be developed.

The procedure used is the same as that employed for the dc-dc converter. The resonant converter is treated as a two-port network, and a state model is written with the port voltages as the inputs. The transistors and diodes are modeled by piecewise linear resistors. The values of resistance employed are calculated from the manufacturer's data sheet for that particular device.

As an illustration, the state model for the parallel-loaded resonant converter is developed. This topology is used here because of its voltage source type output and its usage in [15]. The network utilized in the formulation of the state model is given in Figure 3.3. Transistors Q1 and Q4 are represented by resistance R_{T1} with R_{D1} representing diodes D1 and D4. R_{T3} represents transistors Q2 and Q3, and R_{D3} represents diodes D2 and D3. In Figure 3.3, R_L is the series resistance of the inductor, and R_C is the effective series resistance of the capacitor. The state model is given in (3.1). In this equation, $\alpha_{13} = R_{T3}R_{D3}(R_{T1} + R_{D1}) + R_{T1}R_{D1}(R_{T3} + R_{D3})$. By representing the transistors and diodes with piecewise linear resistors, a single state model describes the behavior of the resonant

converter. The appropriate value of resistance is used in (3.1) depending on whether a device is conducting or blocking.

$$\frac{d}{dt}\begin{bmatrix} i_L \\ v_C \end{bmatrix} = \begin{bmatrix} -\frac{1}{L}\left\{ R_L + \frac{2R_{T1}R_{D1}R_{T3}R_{D3}}{\alpha_{13}} \right\} & 0 \\ 0 & -\frac{1}{R_C C} \end{bmatrix} \begin{bmatrix} i_L \\ v_C \end{bmatrix}$$

$$+ \begin{bmatrix} \frac{1}{L}\left\{ 1 - \frac{2R_{T1}R_{D1}(R_{T3} + R_{D3})}{\alpha_{13}} \right\} & -\frac{1}{L} \\ 0 & \frac{1}{R_C C} \end{bmatrix} \begin{bmatrix} v_1 \\ v_2 \end{bmatrix} \qquad (3.1)$$

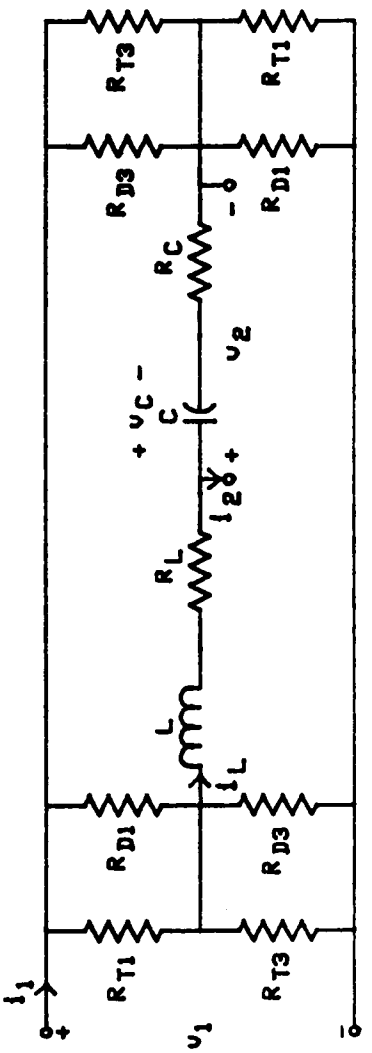

Figure 3.3. Network for formulating state model of parallel-loaded resonant converter.

CHAPTER 4. SIMULATION PROCEDURE

4.1 Introduction

The dynamic response of a spacecraft power system, which is treated as an interconnection of components, may be obtained using two different approaches. In one approach, all component equations are combined to form an overall system model [5]. The spacecraft power system simulation is carried out at the system level using this system model. A second approach is employed here. The simulation is performed at the component level. The state model for each component is solved independently of other components. The coupling between components is accounted for through the state model inputs.

This chapter is divided into three parts. The first part develops the recursive relation used to solve the state model of each component. The alternating solution procedure utilized to solve the system is discussed in the second part. In the third part, the proposed modular state variable approach is compared to performing the simulation at the system level.

4.2 Recursive Relation for the Solution of Component State Models

As previously stated, the spacecraft power system is treated as an interconnection of components. Each component is modeled by a two-port network, and a state model is written. The state variables are associated with any capacitors or inductors located inside the

two-port network, and the inputs to the state model are the port voltages. Therefore, each component is represented by a set of equations of the form

$$\dot{\underline{x}} = A\underline{x} + B\underline{u} \tag{4.1}$$

where $\underline{x}$ is a vector of state variables, $\underline{u}$ is a vector of inputs, and A and B are matrices.

The recursive relation utilized to solve the state model of each component is developed beginning with (4.1) and is a modification of the approach used in [29]. For a continuous system, the solution to (4.1) is given by

$$\underline{x}(t) = \Phi(t)\underline{x}(0) + \int_0^t \Phi(t-\tau)B\underline{u}(\tau)\, d\tau \tag{4.2}$$

where $\Phi(t)$ is the state transition matrix and $\underline{x}(0)$ is a vector containing the initial values of the state variables. Equation (4.2) is valid if the A and B matrices are constant. However, in the simulation of a device such as a power converter, the entries in the A and B matrices are not constant because they depend on which switching devices are blocking and which are conducting. Also, and more importantly, the vector of inputs $\underline{u}$ may now contain entries which are unknown functions of time, which is a result of modeling the spacecraft power system as an interconnection of modular components. Therefore, the convolution integral in (4.2) is difficult to evaluate.

Since (4.2) cannot be used in its present form, two steps are taken to modify it. First, instead of integrating from 0 to t, the limits of integration are selected such that A and B are constant for that interval. Let the interval [0,T] be an interval which satisfies this condition. The value of the state vector at time t = T can be calculated by

$$\underline{x}(T) = \Phi(T)\underline{x}(0) + \int_0^T \Phi(T-\tau)B\underline{u}(\tau)\, d\tau \tag{4.3}$$

Secondly, in order to evaluate the convolution integral in (4.3), the entries in $\underline{u}$ are assumed constant or clamped for the interval [0,T]. If A is nonsingular, the convolution integral in (4.3) can be replaced by a closed-form expression. Equation (4.3) becomes

$$\underline{x}(T) = \Phi(T)\underline{x}(0) + [\Phi(T) - I]A^{-1}B\underline{u}(0) \tag{4.4}$$

Using (4.4), the value of the state variables at time = (k+1)T can be computed from the value at time = kT using the following recursive relation

$$\underline{x}(k+1) = \Phi(T)\underline{x}(k) + [\Phi(T) - I]A^{-1}B\underline{u}(k) \tag{4.5}$$

The variable T will be referred to as the time step. The selection of a value for T is very critical. It must be small enough so that A and B are constant over the interval [0,T]. Since the

inputs are assumed to be clamped for one time step, T must be chosen small enough so that the inputs do not change appreciably over the interval [0,T].

Before (4.5) can be used, the state transition matrix must be calculated. If the state model for a particular component is of order two, the state transition matrix can be found in closed form. Beginning with

$$A = \begin{bmatrix} a_{11} & a_{12} \\ a_{21} & a_{22} \end{bmatrix} \tag{4.6}$$

the entries in the state transition matrix can be expressed in terms of a_{11}, a_{12}, a_{21}, and a_{22} by finding the inverse Laplace transform of the matrix $[sI - A]^{-1}$. The determinant of matrix $[sI - A]$ is the characteristic equation. Depending on the roots of this equation, $\Phi(t)$ can have three different forms corresponding to an underdamped, overdamped, or critically damped system. $\Phi(T)$ is calculated by setting $t = T$. For higher order state models, $\Phi(T)$ can be calculated using a power series [30].

Each component in the spacecraft power system is represented by an equation like (4.5). Before simulation begins, the matrices $\Phi(T)$ and $[\Phi(T) - I]A^{-1}B$ are calculated. If A is singular, the matrix $[\Phi(T) - I]A^{-1}B$ can still be calculated. The matrix $[\Phi(T) - I]A^{-1}$ is

first calculated using the following power series

$$[\Phi(T) - I]A^{-1} = IT + \frac{AT^2}{2!} + \frac{A^2T^3}{3!} + \frac{A^3T^4}{4!} + \ldots \qquad (4.7)$$

The matrix obtained from (4.7) is then post-multiplied by B to yield $[\Phi(T) - I]A^{-1}B$. For a component state model of order three or more, equation (4.7) is utilized to first calculate $[\Phi(T) - I]A^{-1}$. This matrix is then multiplied by the A matrix and added to the identity matrix to form the state transition matrix. This calculation is verified by multiplying (4.7) by A and adding the identity matrix to the results which yields the power series for $\Phi(T)$

$$\Phi(T) = e^{AT} = I + AT + \frac{(AT)^2}{2!} + \frac{(AT)^3}{3!} + \ldots \qquad (4.8)$$

For devices such as power converters, a set of matrices $[\Phi(T) - I]A^{-1}B$ and $\Phi(T)$ exists for each interval of operation. For example, three sets of these matrices are required to simulate a dc-dc converter. During simulation, the matrices corresponding to a particular operating interval are used to calculate $\underline{x}(k+1)$ when the converter operates in that interval. The calculation of $\underline{x}(k+1)$ requires two multiplications of a matrix and a vector and one vector addition. Since the dimensions of $\underline{x}$ and $\underline{u}$ are small, this calculation is computationally fast.

4.3 System Simulation Procedure

The state model of each component is solved using (4.5). An alternating solution method is employed to simulate the entire system [6]. The solution procedure alternates between updating the state variables for each component and recalculating the inputs for all components. This procedure is discussed in this section.

Examination of (4.5) indicates that the state variables at time = (k+1)T are calculated from those at time = kT and the inputs at time = kT. The inputs to each state model are the port voltages. With these voltages known for each time step, the calculation of the new value of the state variables proceeds as if all two ports are decoupled. This is a result of modeling each component as a two-port network and writing a state model with the port voltages as the inputs. Since the state equations of each component are solved independently of all other components, a different time step T could be used for different components if desired. In addition, parallel processing could be utilized to speed up computation.

After the state variables for all components have been updated, the inputs must be recalculated. This calculation is performed with all two ports interconnected. All inductors are replaced by ideal current sources with a value equal to the current flowing through the inductor at time = kT. A voltage source is substituted for each capacitor; the voltage of this source is equal to the capacitor voltage at time = kT. The inputs are then calculated using network

analysis principles. The coupling between two-port networks is accounted for in this calculation.

In summary, the simulation of the entire system proceeds as follows. At time = kT, $\underline{x}(k)$ and $\underline{u}(k)$ are known, and $\underline{x}(k+1)$ is calculated using (4.5) which assumes that the inputs, $\underline{u}(k)$, are clamped. The inputs for the next time step, $\underline{u}(k+1)$, are then calculated from the state vector $\underline{x}(k+1)$ of all components using network analysis principles. This process of alternately solving the dynamic equations of each component and the inputs for all components continues until the end of the simulation.

4.4 Comparison to Other Formulations

The proposed modular state variable approach has been presented in the previous two sections. This approach will be compared to two other formulations in this section. In the first formulation, a state model is developed for the entire system. The only inputs in this state model are known functions of time. For the second formulation, all component state models are combined together into one state model.

One of the assumptions made in the modular state variable approach is that the inputs to each component are clamped for each time step. The state model of components with inputs which are unknown functions of time can be solved using this approximation. The selection of the time step is very critical in using this approximation. If, however, the state model of the system is

developed with only inputs which are known functions of time, this approximation is unnecessary. Using this approach, the state model for the entire system would be

$$\dot{\underline{x}}_s = A_s \underline{x}_s + B_s \underline{u}_s \tag{4.9}$$

$$\underline{y}_s = C_s \underline{x}_s + D_s \underline{u}_s \tag{4.10}$$

where the s subscript denotes system. In (4.9), $\underline{x}_s$ is the state vector for the entire system, and $\underline{u}_s$ is the input vector for the entire system. All entries in $\underline{u}_s$ are known functions of time. For a large system, the dimension of $\underline{x}_s$ is quite large, and, therefore, the matrices A_s and B_s are large. Equation (4.10) is utilized to calculate various output quantities such as the voltage or current at some point in the system. Since $\underline{x}_s$ and $\underline{u}_s$ are large, C_s and D_s are also large.

The dynamic response of the system represented by (4.9) and (4.10) may be obtained using the state transition matrix or other numerical algorithm. Recall that the spacecraft power system will contain many power converters which are nonlinear devices. Using the piecewise linear model for switching devices presented here, the entries in A_s, B_s, C_s, and D_s will be dependent on the state of all

switching devices. Therefore, entries in these matrices may have to be recalculated at each time step. For a large system, this would be a time-consuming operation. In the proposed modular state variable approach, all matrices are calculated before simulation begins.

The solution to (4.9) can be obtained using the state transition matrix. Equation (4.3) or some modification to (4.3) such as (4.5) could be utilized. Regardless of the expression used, the state transition matrix must be calculated. Since the dimensions of A_s are large, it must be evaluated using a power series. In addition, it will have to be reevaluated each time A_s changes. The convolution integral will also have to be recalculated each time A_s or B_s changes. If (4.5) is employed, the matrix $[\Phi(T) - I]A^{-1}B$ must be recalculated each time A_s or B_s changes. Therefore, the computation time will increase very rapidly with increasing system size.

Instead of a formulation in which the inputs of the state model are known functions of time, all component state equations can be combined into one large system model. This model differs from the one presented in (4.9) and (4.10) in that all inputs are not known functions of time. Thus, in the solution of the system, the time variation of some of the inputs must be assumed. If the time step is selected properly, these inputs may be assumed constant for each time step. Since this is the same assumption made in the modular state variable approach, it can be shown that this formulation is the same as the modular state variable approach. Three example systems are

utilized to illustrate this point.

The first example consists of n two-port networks connected in series as shown in Figure 4.1. Notice that the output voltage of one two-port network is the input voltage to the next. The state model for two-port #1 is

$$\dot{\underline{x}}_1 = A_1\underline{x}_1 + B_1\underline{u}_1 \tag{4.11}$$

where $\underline{u}_1 = \begin{bmatrix} v_{11} \\ v_{12} \end{bmatrix}$,

and the state model for the second two-port is

$$\dot{\underline{x}}_2 = A_2\underline{x}_2 + B_2\underline{u}_2 \tag{4.12}$$

where $\underline{u}_2 = \begin{bmatrix} v_{21} \\ v_{22} \end{bmatrix}$

Since $v_{12} = v_{21}$, B_1 and B_2 are partitioned as follows

$$B_1 = [B_{11} \quad B_{12}] \tag{4.13}$$

$$B_2 = [B_{21} \quad B_{22}] \tag{4.14}$$

B_{11} is the submatrix of B_1 which is multiplied by v_{11}, and B_{12} is the submatrix of B_1 which is multiplied by v_{12}.

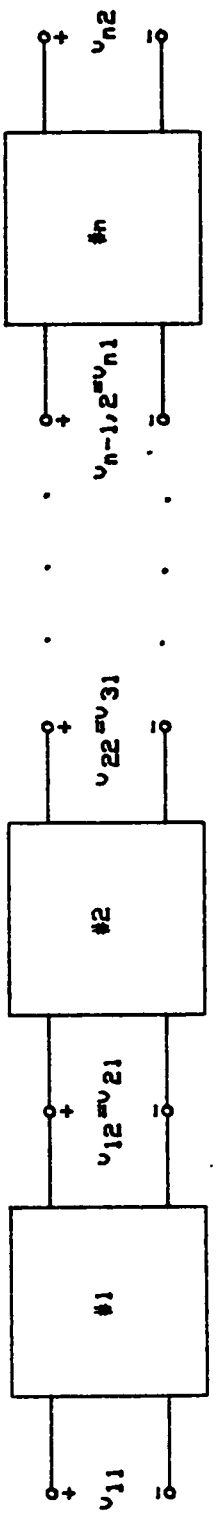

Figure 4.1. N two-port networks connected in series.

The state equations of all n two-ports are combined into one system model represented by (4.9). For this case,

$$A_s = \begin{bmatrix} A_1 & & & & & \\ & A_2 & & & & \\ & & A_3 & & & \\ & & & \ddots & & \\ & & & & \ddots & \\ & & & & & A_n \end{bmatrix} \tag{4.15}$$

$$B_s = \begin{bmatrix} B_{11} & B_{12} & & & & \\ & B_{21} & B_{22} & & & \\ & & B_{31} & B_{32} & & \\ & & & \ddots & \ddots & \\ & & & & \ddots & \ddots \\ & & & & B_{n1} & B_{n2} \end{bmatrix} \tag{4.16}$$

$$\underline{x}_s = \begin{bmatrix} \underline{x}_1 \\ \underline{x}_2 \\ \cdot \\ \cdot \\ \cdot \\ \cdot \\ \cdot \\ \underline{x}_n \end{bmatrix} \qquad \underline{u}_s = \begin{bmatrix} v_{11} \\ v_{12} \\ v_{22} \\ v_{32} \\ \cdot \\ \cdot \\ \cdot \\ \cdot \\ v_{n-1,2} \\ v_{n2} \end{bmatrix} \tag{4.17}$$

Only the nonzero submatrices in A_s and B_s are given in (4.15) and (4.16).

This set of equations can be solved using (4.2). A_s is a block diagonal matrix as seen in (4.15). Using linear system theory, a function of a block diagonal matrix may be computed by calculating the matrix function of each diagonal block [50,51]. Therefore, the state transition matrix for the system equation can be calculated by calculating the state transition matrix of each diagonal block using (4.8). The state transition matrix for the system equation is

$$\Phi_s(T) = \begin{bmatrix} \Phi_1(T) & & & & \\ & \Phi_2(T) & & & \\ & & \Phi_3(T) & & \\ & & & \ddots & \\ & & & & \Phi_n(T) \end{bmatrix} \tag{4.18}$$

The convolution integral in (4.2) is

$$\int_{kT}^{(k+1)T} \Phi_s(t-\tau)B_s\underline{u}_s(\tau)\, d\tau \tag{4.19}$$

Assuming that all entries in $\underline{u}_s$ are constant, this integral can be replaced by

$$[\Phi_s(T) - I_s]A_s^{-1}B_s\underline{u}_s \tag{4.20}$$

I_s is an identity matrix which contains identity submatrices on its diagonal. A_s is nonsingular if all of its submatrices are nonsingular. The matrix $[\Phi_s(T) - I_s]A_s^{-1}$ is

$$\begin{bmatrix} [\Phi_1(T) - I_1]A_1^{-1} & & & \\ & [\Phi_2(T) - I_2]A_2^{-1} & & \\ & & \ddots & \\ & & & [\Phi_n(T) - I_n]A_n^{-1} \end{bmatrix} \tag{4.21}$$

Let $[\Phi_i(t) - I_i]A_i^{-1}$ be Θ_i. Post-multiplication of (4.21) by B_s yields

$$\begin{bmatrix} \Theta_1 B_{11} & \Theta_1 B_{12} & & & \\ & \Theta_2 B_{21} & \Theta_2 B_{22} & & \\ & & \ddots & & \\ & & & \Theta_n B_{n1} & \Theta_n B_{n2} \end{bmatrix} \tag{4.22}$$

Examination of (4.18) and (4.22) reveals that these equations are the same as those used in the modular state variable approach. The state transition matrix of each two-port network appears on the diagonal of (4.18). Notice in (4.22) that Θ_1 multiplies only the submatrices of B_1. Therefore, the state equations of each two-port network are solved independently of the other two-port networks.

In the second example, n two-port networks are connected in parallel as seen in Figure 4.2. Notice that there are only two inputs to the system. The state model for the i_{th} component is given by

$$\dot{\underline{x}}_i = A_i \underline{x}_i + B_i \underline{u} \tag{4.23}$$

The vector $\underline{u}$ contains the two inputs.

The state equations for all components are combined into one system model as was done in the first example. A_s and $\underline{x}_s$ are given by (4.15) and (4.17). B_s has the following form

$$B_s = \begin{bmatrix} B_1 \\ B_2 \\ . \\ . \\ . \\ B_n \end{bmatrix} \tag{4.24}$$

The state transition matrix $\Phi_s(T)$ and $[\Phi_s(T) - I_s]A_s^{-1}$ are given by (4.18) and (4.21), respectively. Again let $[\Phi_i(T) - I_i]A_i^{-1}$ be Θ_i and post-multiply (4.21) by (4.24). The resulting matrix is

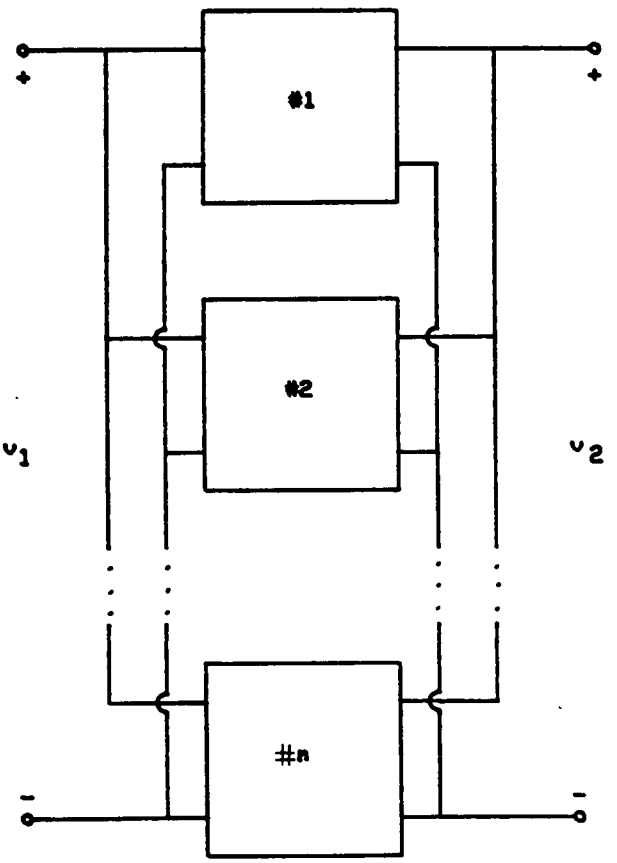

Figure 4.2. N two-port networks connected in parallel.

$$\begin{bmatrix} \theta_1 B_1 & & & & \\ & \theta_2 B_2 & & & \\ & & \theta_3 B_3 & & \\ & & & \ddots & \\ & & & & \theta_n B_n \end{bmatrix} \tag{4.25}$$

Equations (4.18) and (4.25) are the same as those of the modular state variable approach because of the decoupling which exists between two-port networks.

The first two example systems considered all components connected in series and parallel. The simple system shown in Figure 4.3, which consists of two components in parallel connected in series with two more components, is used for the third example system. The component state models are

Component #1

$$\dot{\underline{x}}_1 = A_1 \underline{x}_1 + [B_{11} \quad B_{12}] \begin{bmatrix} \\ v_1 \\ v_2 \end{bmatrix} \tag{4.26}$$

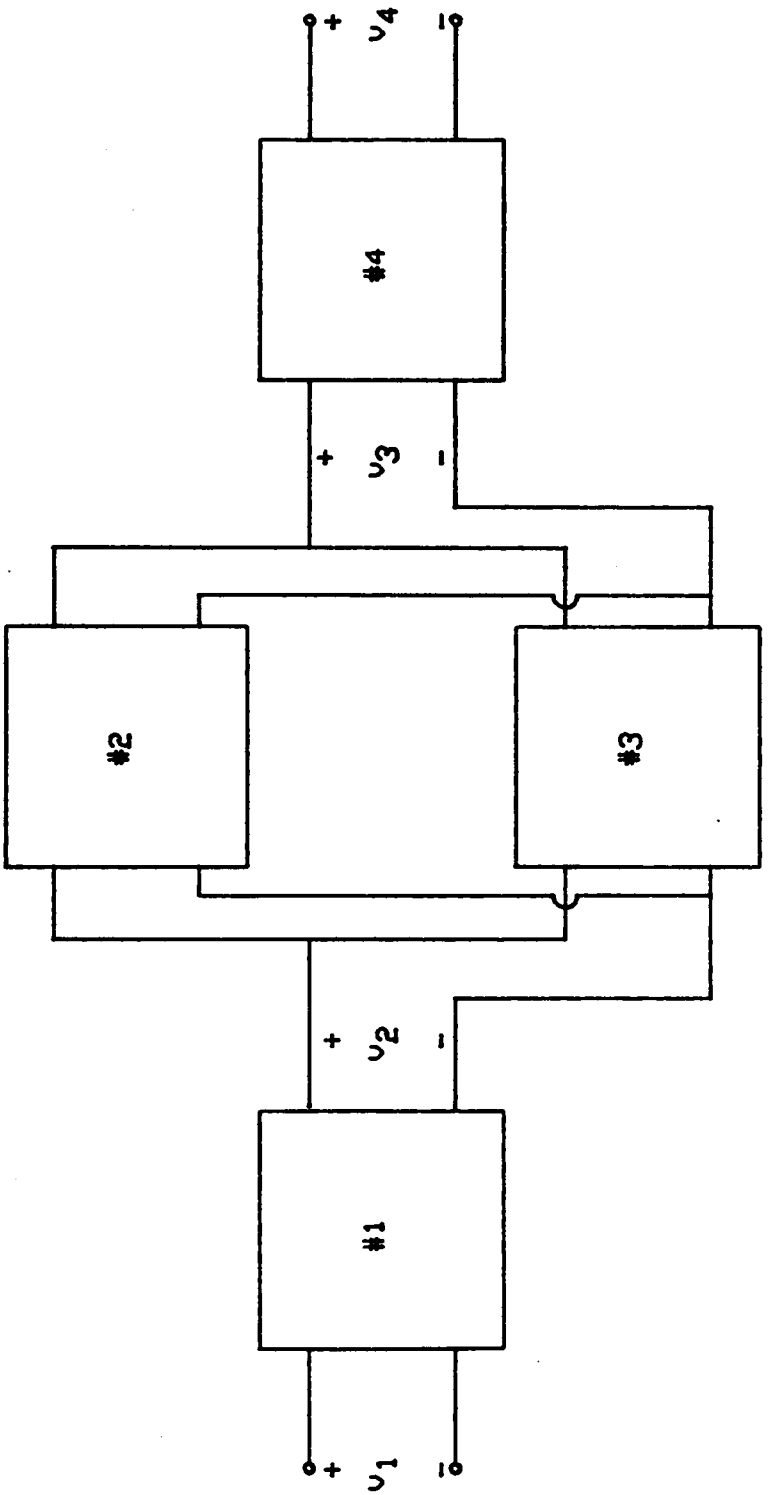

Figure 4.3. 2 two-port networks in parallel connected in series with 2 two-port networks.

Component #2

$$\dot{\underline{x}}_2 = A_2\underline{x}_2 + \begin{bmatrix} B_{21} & B_{22} \end{bmatrix} \begin{bmatrix} v_2 \\ v_3 \end{bmatrix} \tag{4.27}$$

Component #3

$$\dot{\underline{x}}_3 = A_3\underline{x}_3 + \begin{bmatrix} B_{31} & B_{32} \end{bmatrix} \begin{bmatrix} v_2 \\ v_3 \end{bmatrix} \tag{4.28}$$

Component #4

$$\dot{\underline{x}}_4 = A_4\underline{x}_4 + \begin{bmatrix} B_{41} & B_{42} \end{bmatrix} \begin{bmatrix} v_3 \\ v_4 \end{bmatrix} \tag{4.29}$$

Combining (4.26)-(4.29) into the form of (4.9) yields

$$A_S = \begin{bmatrix} A_1 & & & \\ & A_2 & & \\ & & A_3 & \\ & & & A_4 \end{bmatrix} \tag{4.30}$$

$$B_S = \begin{bmatrix} B_{11} & B_{12} & & \\ & B_{21} & B_{22} & \\ & B_{31} & B_{32} & \\ & & B_{41} & B_{42} \end{bmatrix} \tag{4.31}$$

$$\underline{x}_S = \begin{bmatrix} \underline{x}_1 \\ \underline{x}_2 \\ \underline{x}_3 \\ \underline{x}_4 \end{bmatrix} \qquad \underline{u}_S = \begin{bmatrix} v_1 \\ v_2 \\ v_3 \\ v_4 \end{bmatrix} \tag{4.32}$$

The matrices for this system may be found by letting n = 4 in (4.18) and (4.21). Post-multiplication of (4.21) with n = 4 by (4.31) produces

$$\begin{bmatrix} \theta_1 B_{11} & \theta_1 B_{12} & & \\ & \theta_2 B_{21} & \theta_2 B_{22} & \\ & \theta_3 B_{31} & \theta_3 B_{32} & \\ & & \theta_4 B_{41} & \theta_4 B_{42} \end{bmatrix} \tag{4.33}$$

Notice again that each state model is solved independent of the other state models which is exactly the modular state variable approach.

In summary, these examples have demonstrated that combining all component equations in an overall system model produces the same equations as the modular state variable approach. This is a result of treating each component as a two-port network and writing a state model with the port voltages as the inputs. The A matrix of each two-port network is independent of the A matrix for all other two-port networks. The component state models are coupled through the inputs. Utilization of the modular state variable approach is similar to employing sparse matrix techniques because only the submatrices given in (4.18) and (4.22) or (4.25) are stored during computer simulation.

CHAPTER 5. SIMULATION OF EXAMPLE SYSTEMS

5.1 Introduction

A modular state variable approach for the simulation of spacecraft power systems has been presented in the previous chapters. Three example systems are simulated using this approach and SPICE2 [4]. A comparison of the simulations shows that the two approaches predict approximately the same dynamic response. However, the modular state variable approach is more computationally efficient because it uses less CPU time than SPICE2.

In order to simulate realistic systems, power bipolar transistors and power diodes are utilized in all converters. The bipolar transistors are manufactured by Westinghouse and are qualified for space flight. Utilization of these transistors in the converters required the determination of model parameters for the SPICE2 bipolar transistor model. This model has 40 parameters with certain default values. After careful study, those parameters considered critical for high power bipolar transistors were identified. Most of these parameters are not readily available on the manufacturer's data sheet and have to be measured in the laboratory. SPICE2 also has a diode model with 14 parameters. All necessary diode parameters were obtained from manufacturer's data sheets.

5.2 Example System #1

The first example system is a 20 kHz ac spacecraft power system. It consists of a series resonant converter connected to a transmission line supplying a bridge rectifier load as seen in Figure 5.1. The state model for the parallel-loaded series resonant converter is given in (3.1). A t-model is used for the transmission line, as seen in Figure 5.2, instead of a pi-model. A pi-model cannot be used because the port voltages, which are the voltages across the capacitors in the pi-model, are clamped for each time step. The state model for the transmission line using the circuit in Figure 5.2 is

$$\frac{d}{dt}\begin{bmatrix} i_{L1} \\ i_{L2} \\ v_C \end{bmatrix} = \begin{bmatrix} -\frac{R}{L} & 0 & -\frac{1}{L} \\ 0 & -\frac{R}{L} & \frac{1}{L} \\ \frac{1}{C} & -\frac{1}{C} & 0 \end{bmatrix} \begin{bmatrix} i_{L1} \\ i_{L2} \\ v_C \end{bmatrix} + \begin{bmatrix} -\frac{1}{L} & 0 \\ 0 & -\frac{1}{L} \\ 0 & 0 \end{bmatrix} \begin{bmatrix} v_1 \\ v_2 \end{bmatrix} \qquad (5.1)$$

In Figures 5.1 and 5.2 and equation (5.1), R is one-half of the total line resistance, L is one-half of the total line inductance, and C is the total line capacitance. Figure 5.3 shows a bridge rectifier with output filter capacitor and the circuit used in writing the state model. R_C is the esr of the output filter capacitor. The state model

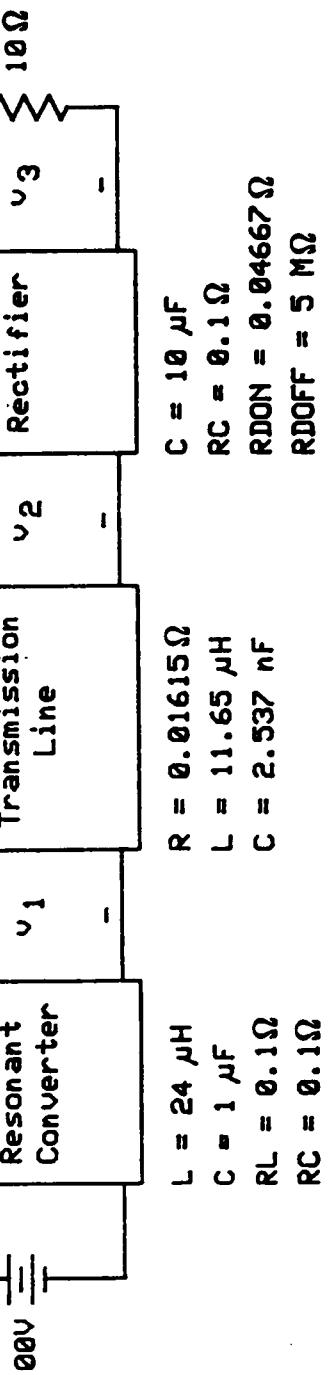

Figure 5.1. Example system #1.

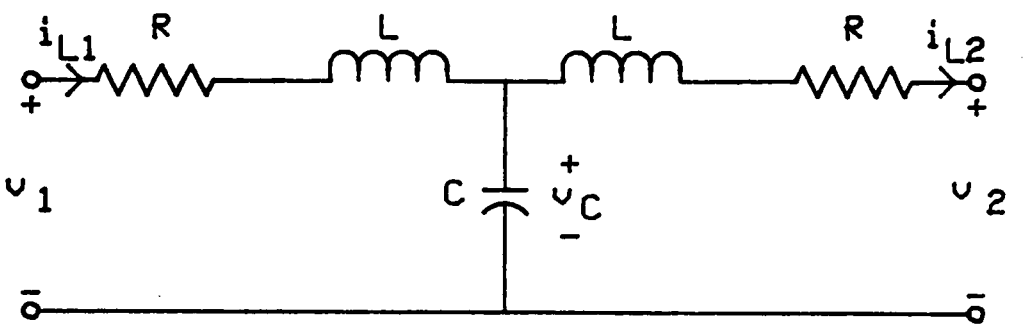

Figure 5.2. Transmission line model.

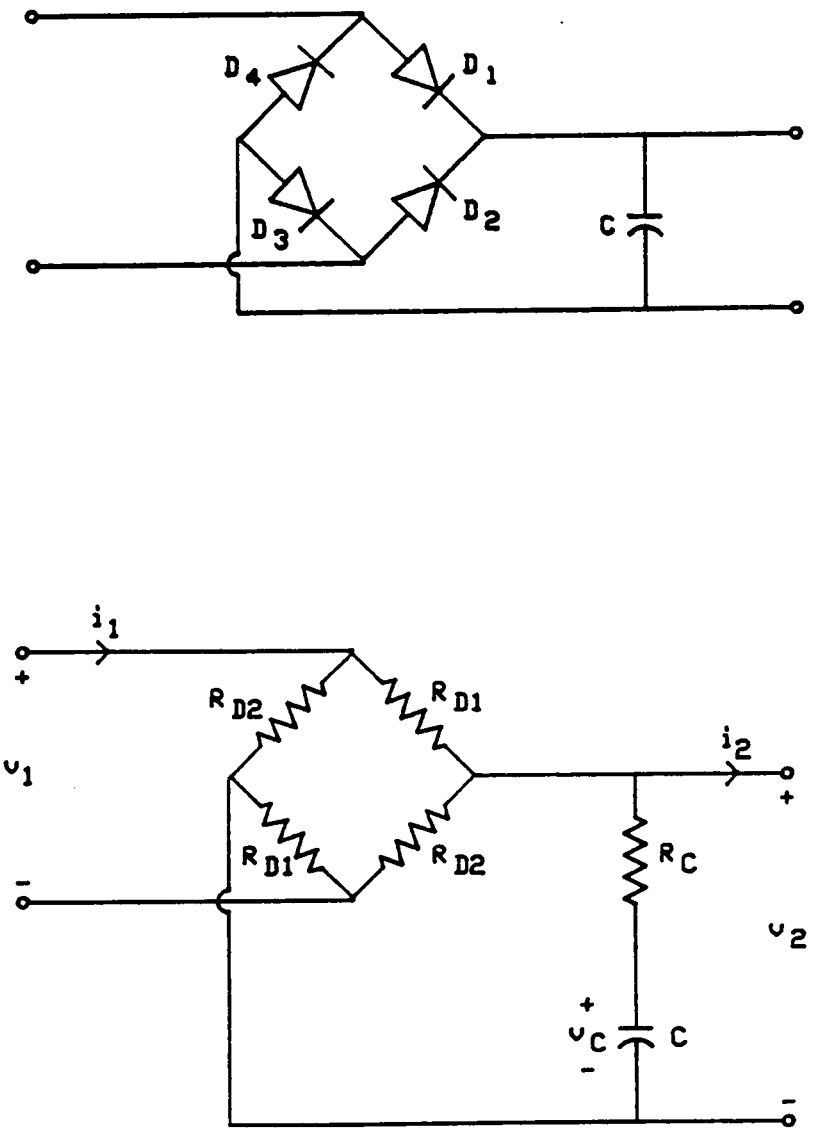

Figure 5.3. Bridge rectifier and its two-port network model.

for the rectifier is

$$\frac{dv_C}{dt} = \frac{-1}{R_C C} v_C + \frac{1}{R_C C} v_2 \qquad (5.2)$$

The transistors used in the resonant converter are Westinghouse D60T804005. This transistor has a collector-emitter sustaining voltage of 800 V and a collector current rating of 100 A (continuous). In order to use the state model in (3.1), the "on" and "off" resistances of this transistor must be determined. Using the manufactuer's data sheet, the "on" resistance and "off" resistance are calculated to be 0.0625 Ω and 400 kΩ, respectively. The part number for the diodes is 1N3913. The current-carrying capacity of these diodes is 30 A (continuous), and the peak inverse voltage is 400 V. The "on" resistance of the diodes is 0.04667 Ω, and the "off" resistance is 5 MΩ. All element values for the resonant converter, transmission line, and rectifier are given below:

Resonant Converter

$R_L = 0.1\Omega$ $\quad L = 24\ \mu H$

$R_C = 0.1\Omega$ $\quad C = 1\ \mu F$

$R_{T(ON)} = 0.0625\ \Omega$ $\quad R_{T(OFF)} = 400\ k\Omega$

$R_{D(ON)} = 0.04667\ \Omega$ $\quad R_{D(OFF)} = 5\ M\Omega$

Transmission Line

$R = 0.01615\ \Omega \quad L = 11.65\ \mu H \quad C = 2.537\ nF$

Rectifier

$R_{D(ON)} = 0.04667\ \Omega \quad R_{D(OFF)} = 5\ M\Omega$

$C = 10\ \mu F \quad R_C = 0.1\ \Omega$

The values of L and C for the resonant converter are given in [31]. The transmission line is 50 m of coaxial cable. The dc source has a value of 100 V and the load is 10 Ω. The SPICE2 parameters for the bipolar transistor and diode are given in Tables 5.1 and 5.2. A description of these parameters may be found in [4].

The port voltages in Figure 5.1 are calculated using the following equations:

$$v_1 = R_{CI}(i_{LI} - i_{L1T}) + v_{CI} \tag{5.3}$$

$$v_2 = 2R_{D(ON)}\ i_{L2T} \pm v_3 \tag{5.4}$$

$$v_3 = \frac{R}{R_{CR}+R}\ v_{CR} + \frac{R_{CR}R}{R_{CR}+R}\ i_{L2T} \tag{5.5}$$

In these equations, the subscripts I, T, and R correspond to inverter, transmission line, and rectifier, respectively. A more exact expression for v_2 may be derived in terms of R_{D1} and R_{D2}. However,

Table 5.1

SPICE2 Transistor Parameters for
Westinghouse P/N D60T804005

Parameter	Value
IS	25 pA
BF	25
NF	1.03
VAF	2000 V
IKF	19.95 A
RB	0.1 Ω
RE	0.005 Ω
RC	0.075 Ω
CJC	9.5 nF
TR	200 ns

Table 5.2

SPICE2 Diode Parameters for
Diode P/N 1N3913

Parameter	Value
RS	0.023 Ω
TT	200 ns
BV	400 V
IBV	80 μA

equation (5.3) is a much simpler expression for v_2. This equation assumes that the two diodes blocking are modeled as open circuits, and the two diodes which are conducting are modeled by the "on" resistance $R_{D(ON)}$. Since v_2 is expressed in terms of v_3, v_3 is always calculated first. Referring to Figure 5.3, the plus sign in (5.4) is used when D1 and D3 conduct, and the minus sign is used when D2 and D4 conduct.

For this simulation, the system is suddenly energized. The transient response for the following 12.5 milliseconds is determined using SPICE2 and the modular state variable approach. The time step used for the modular state variable approach is 0.01 μs. An initial time step of 1 μs is used in SPICE2. However, SPICE2 uses a variable time step method of numerical integration, so the time step varies during simulation. The results of the SPICE2 and modular state variable approach simulations are plotted in Figures 5.4-5.11. Examination of these plots reveals that the modular state variable approach predicts approximately the same response as SPICE2. The modular state variable approach requires one-fifth to one-sixth of the CPU time required by SPICE2 to perform this simulation.

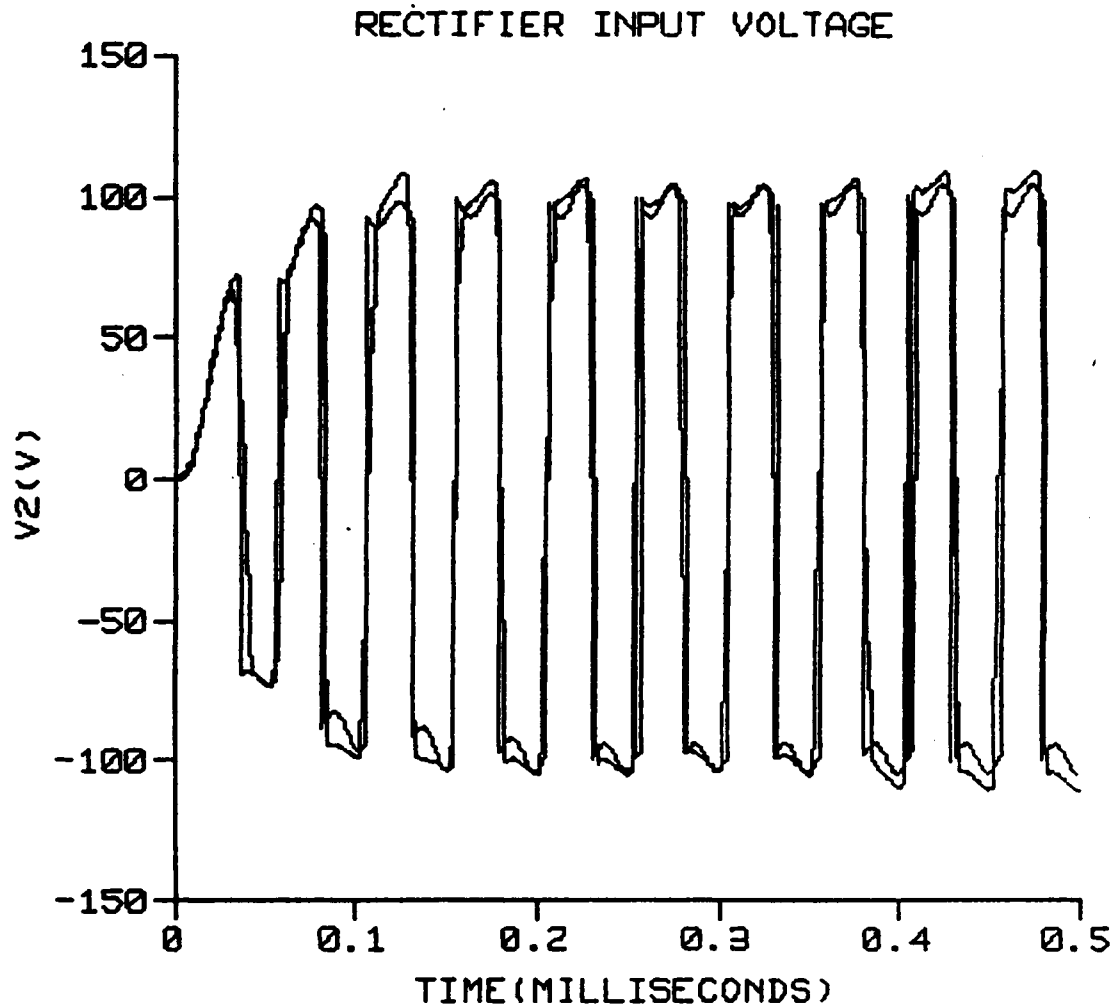

Figure 5.4. Rectifier input voltage for $0 < t < 0.5$ ms.

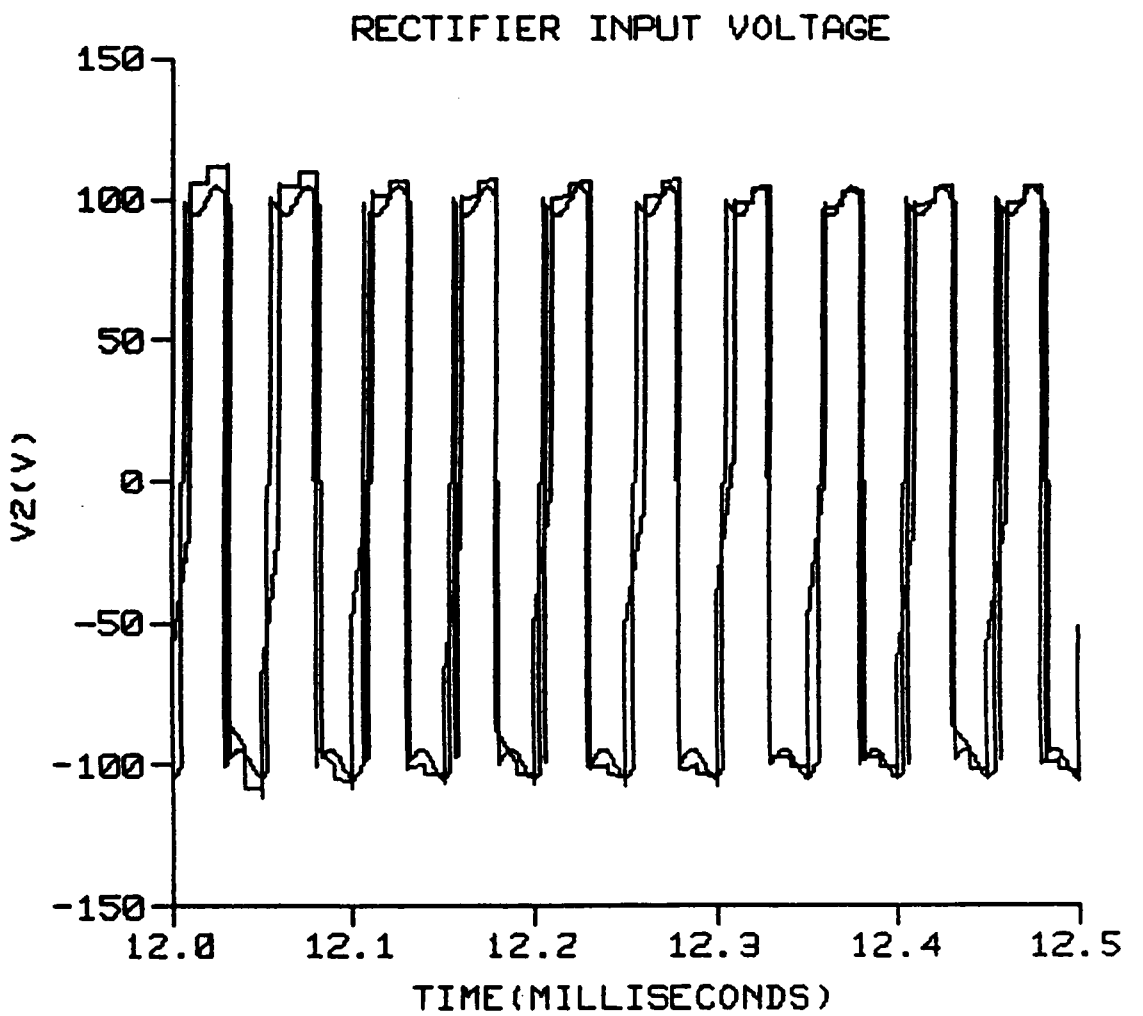

Figure 5.5. Rectifier input voltage for 12 < t < 12.5 ms.

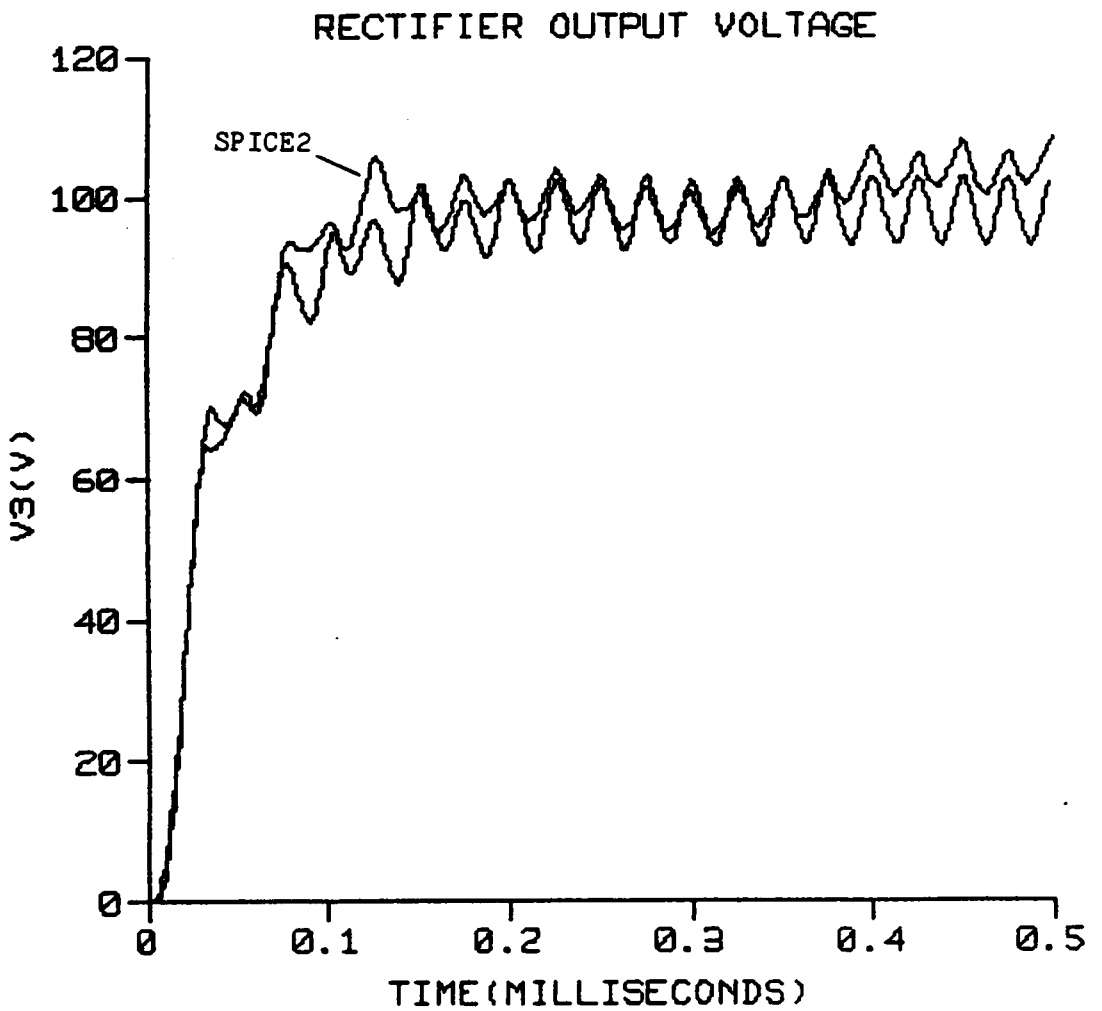

Figure 5.6. Rectifier output voltage for $0 < t < 0.5$ ms.

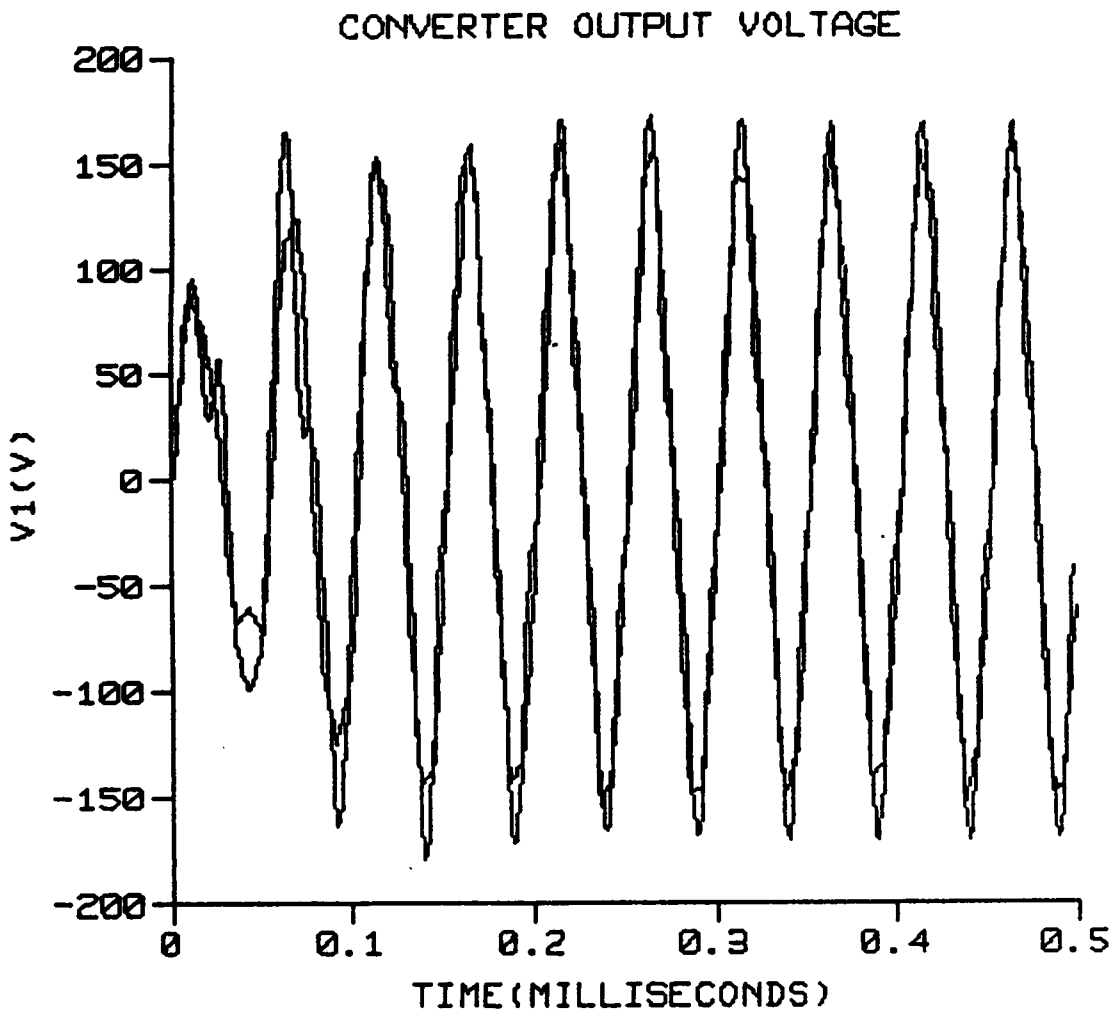

Figure 5.7. Converter output voltage for $0 < t < 0.5$ ms.

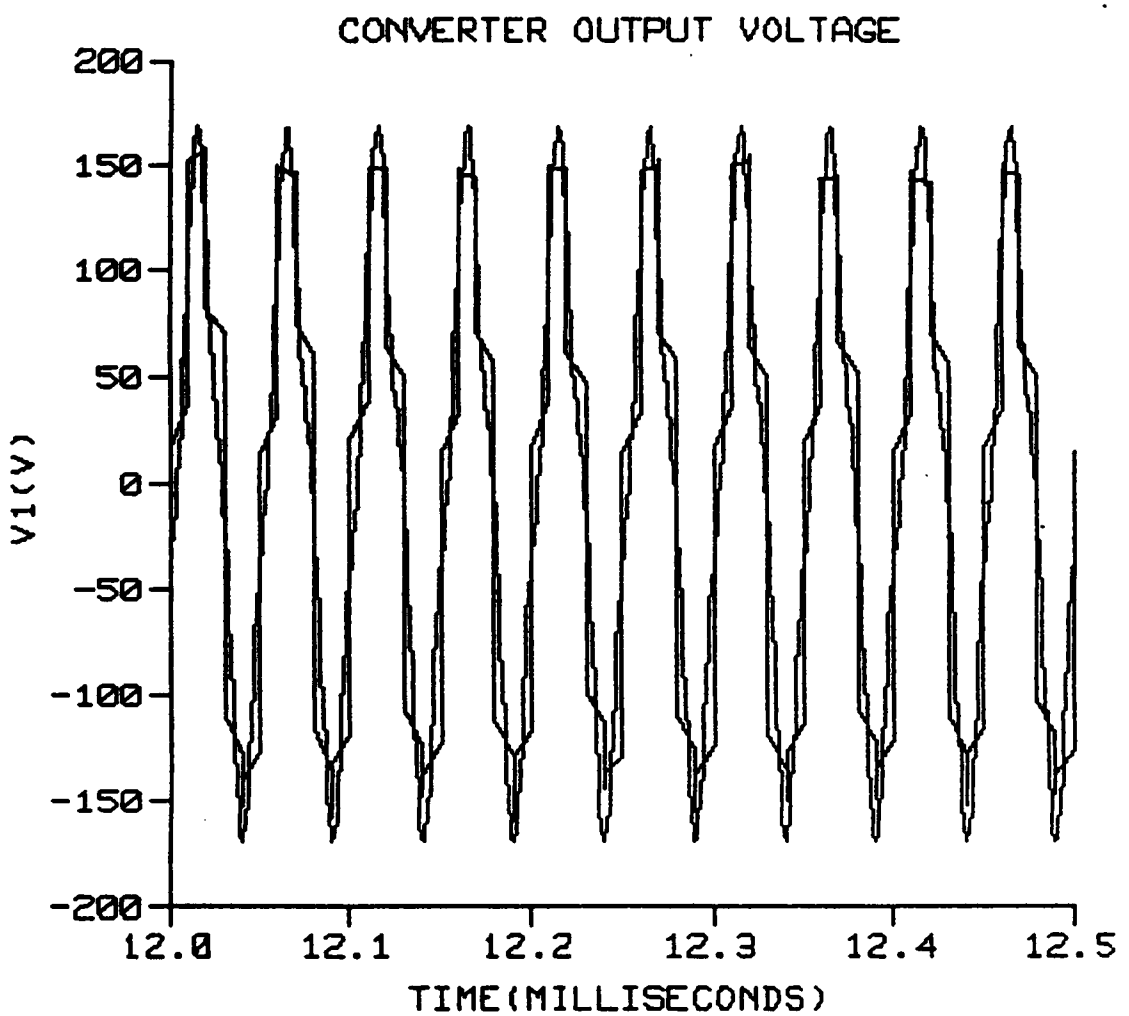

Figure 5.8. Converter output voltage for 12 < t < 12.5 ms.

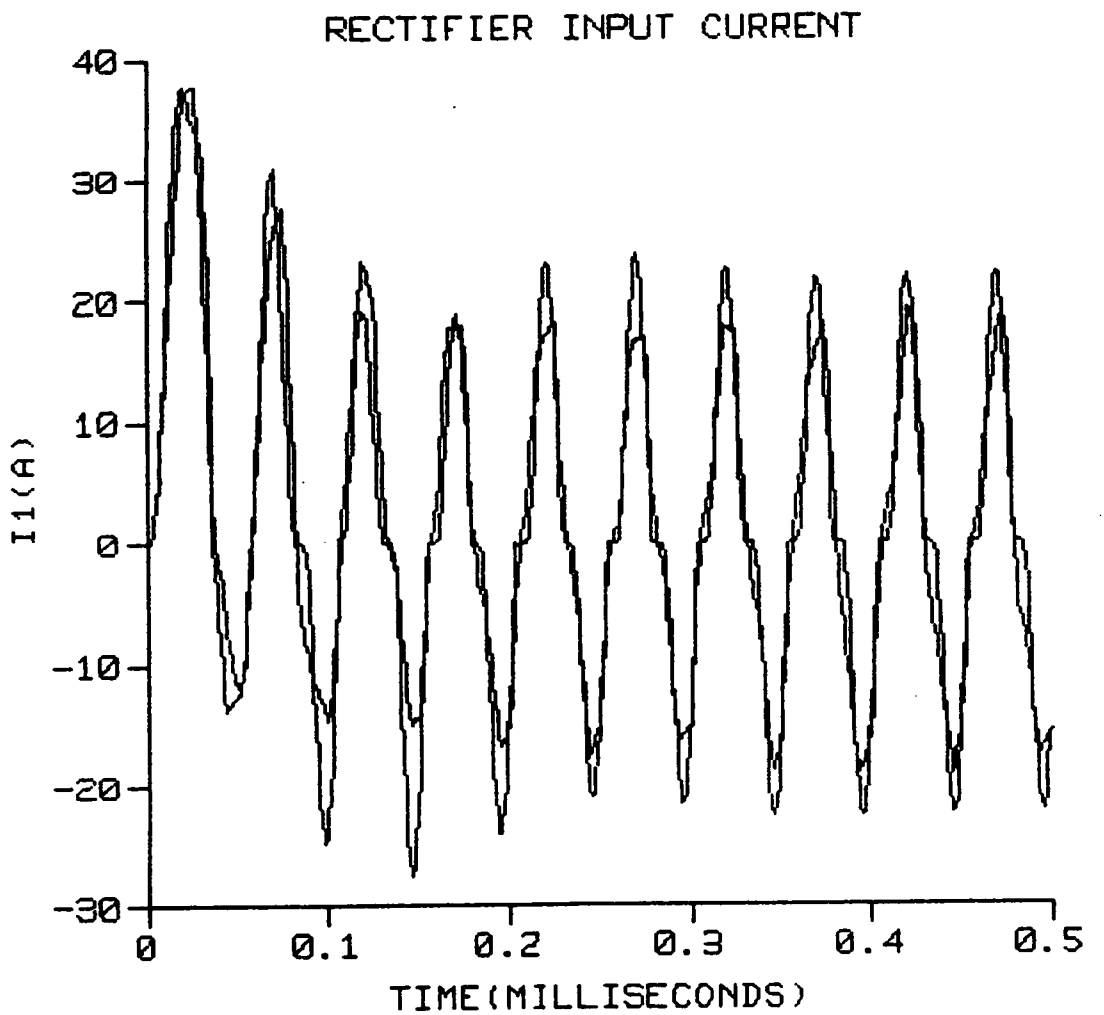

Figure 5.9. Rectifier input current for $0 < t < 0.5$ ms.

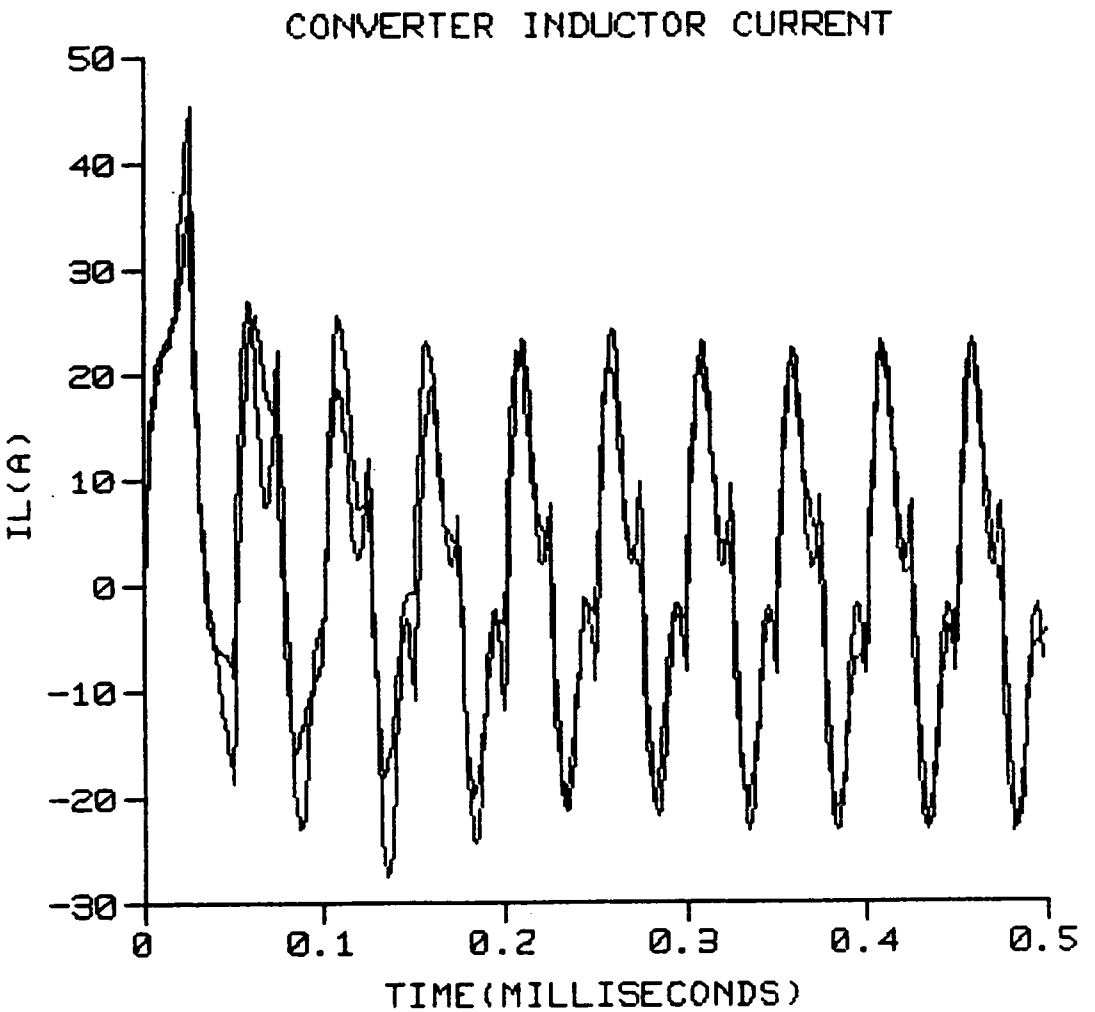

Figure 5.10. Converter inductor current for $0 < t < 0.5$ ms.

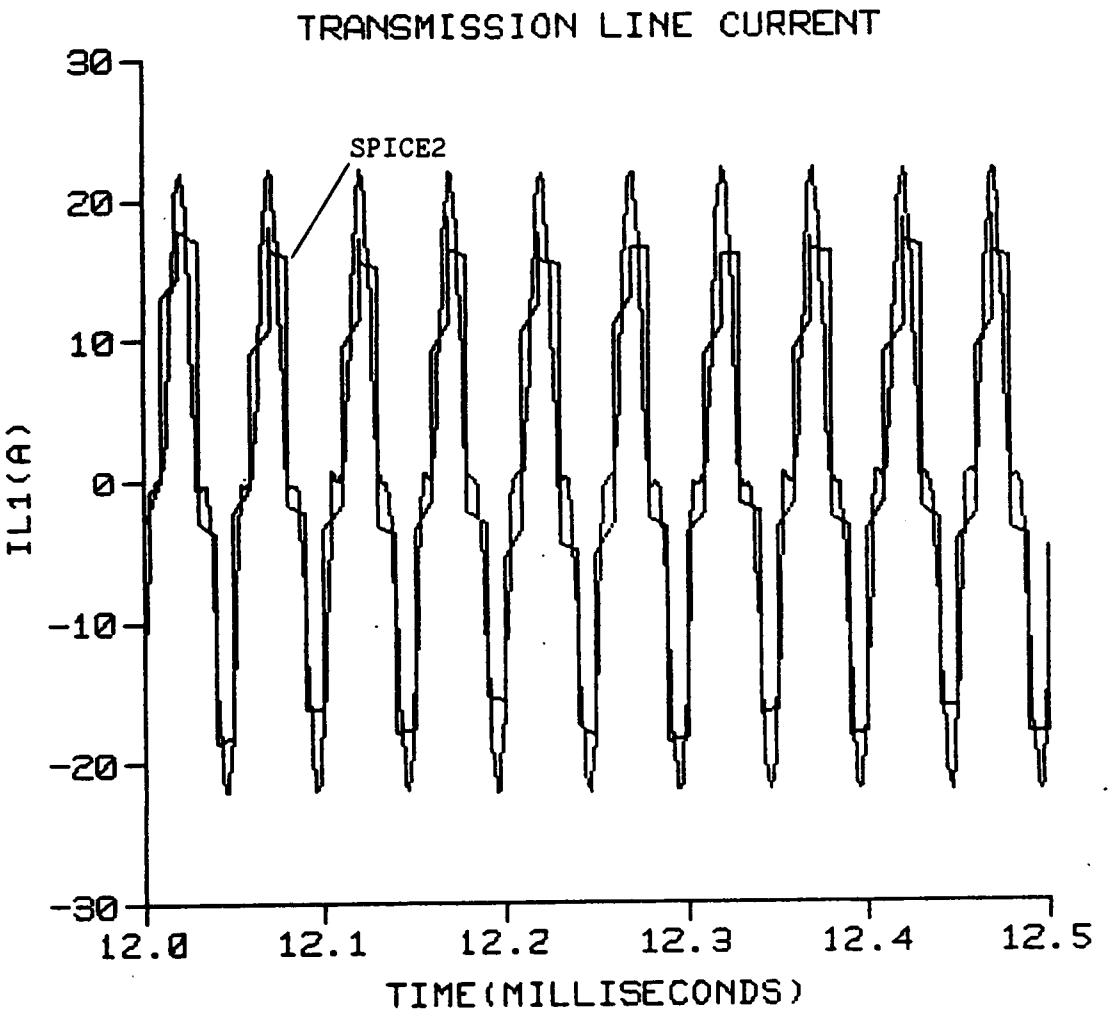

Figure 5.11. Transmission line input current for 12 < t < 12.5 ms.

5.3 Example System #2

The second example system consists of two boost converters connected in series supplying a resistive load as seen in Figure 5.12. The converters are fed from a constant dc source and operated at fixed duty ratios. The state model for the boost converter is given in (2.5). The transistor used in both converters is the Westinghouse D60T804005, which is also used in the series resonant converter in the previous example, with an "on" resistance of 0.0625 Ω and an "off" resistance of 400 kΩ. A 1N3913 diode, which is also used in the previous example, is utilized in the first converter; it has an "on" resistance of 0.04667 Ω and an "off" resistance of 5 MΩ. An MR876 diode, which has a peak inverse voltage of 600 V and a current-carrying capacity of 50 A (continuous), is employed in the second converter. The SPICE2 parameters for this diode are given in Table 5.3. Using the manufacturer's data sheet, the "on" resistance and "off" resistance are calculated to be 0.028 Ω and 12 MΩ, respectively. The other element values for the two converters are

Converter #1	Converter #2
R_{L1} = 0.1 Ω	R_{L2} = 0.1 Ω
L_1 = 1 mH	L_2 = 2.5 mH
R_{C1} = 0.1 Ω	R_{C2} = 0.05 Ω
C_1 = 75 μF	C_2 = 15 μF

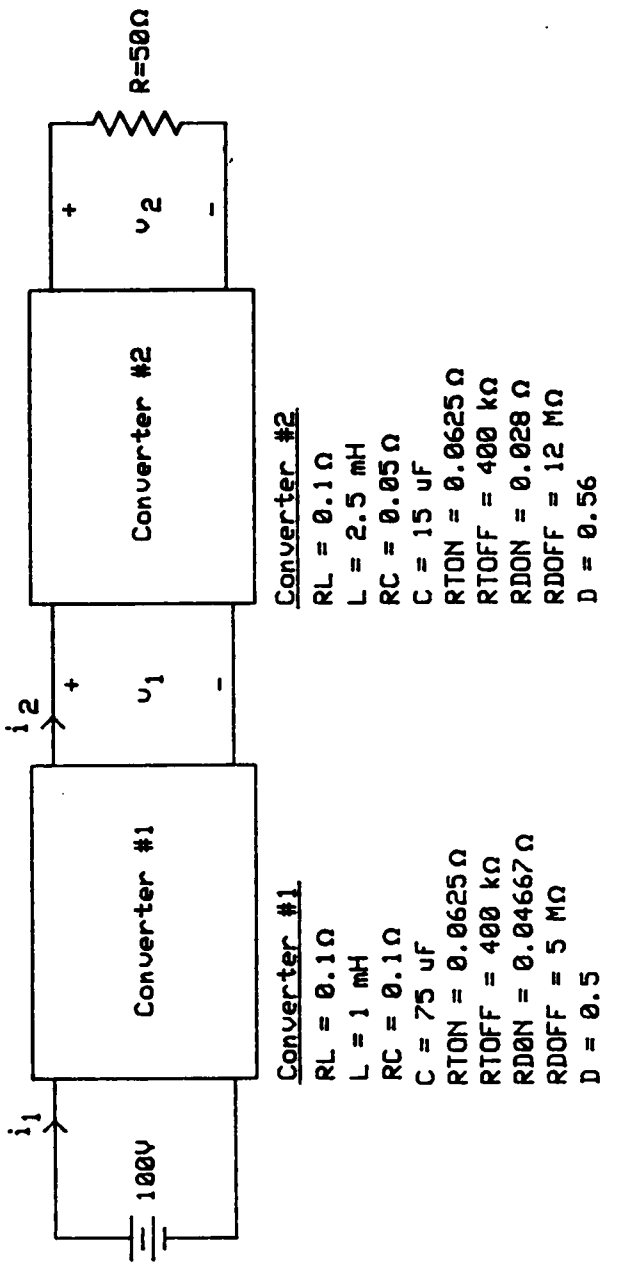

Figure 5.12. Example system #2.

Table 5.3

SPICE2 Diode Parameters for
Diode P/N MR876

Parameter	Value
RS	0.014 Ω
TT	120 ns
BV	600 V
IBV	50 μA

The constant dc source has a value of 100 V and the load is a 50 Ω resistor. Converter #1 is operated at a fixed duty ratio, D_1, of 0.5 while the duty ratio, D_2, of converter #2 is fixed at 0.56.

To illustrate how the inputs are calculated from the state variables of the converters, the equations for calculating v_1 and v_2 in Figure 5.12 are given here. The output voltage of the second converter, v_2, is calculated using

$$v_2 = \frac{RR_{C2}R_{T2}}{R_{C2}(R+R_{T2}+R_{D2})+R(R_{T2}+R_{D2})} i_{L2} + \frac{R(R_{T2}+R_{D2})}{R_{C2}(R+R_{T2}+R_{D2})+R(R_{T2}+R_{D2})} v_{C2} \tag{5.6}$$

For the first converter, the output voltage, which is the input voltage of the second converter, is calculated by

$$v_1 = \frac{R_{T1}R_{C1}}{R_{T1}+R_{C1}+R_{D1}} i_{L1} + \frac{R_{T1}+R_{D1}}{R_{T1}+R_{C1}+R_{D1}} v_{C1} + \frac{R_{C1}(R_{T1}+R_{D1})}{R_{T1}+R_{C1}+R_{D1}} i_{L2} \tag{5.7}$$

In (5.6) and (5.7), variables associated with converter #1 are subscripted with a 1 and those associated with converter #2 with a 2.

The response of this system to the sudden application of the source is simulated using SPICE2 and the modular state variable approach. The output from SPICE2 and the modular state variable approach are plotted together in Figures 5.13-5.20. As can be seen from these figures, the modular state variable approach predicts approximately the same response as SPICE2. For this example, the modular state variable approach requires only one-twentieth of the CPU time required by SPICE2.

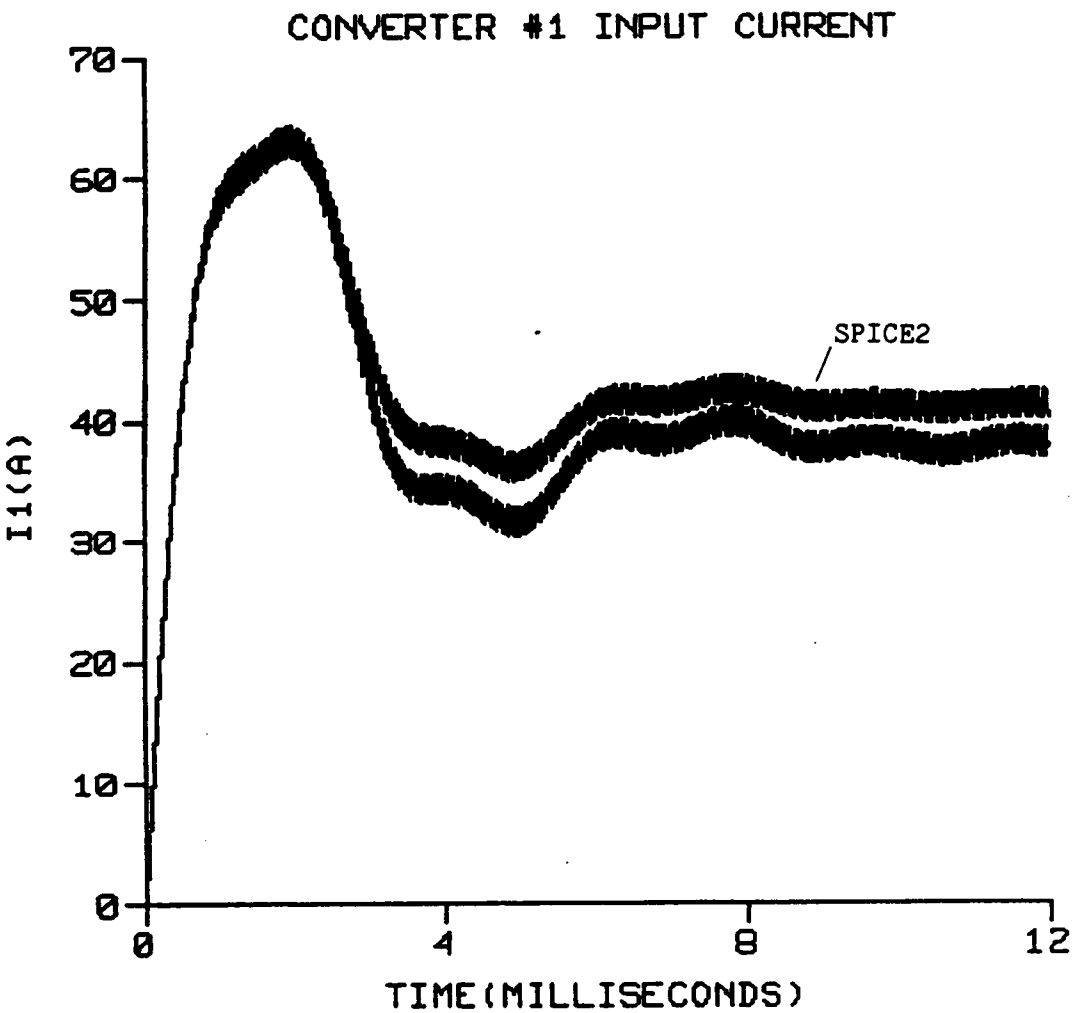

Figure 5.13. Converter #1 input current for $0 < t < 12$ ms.

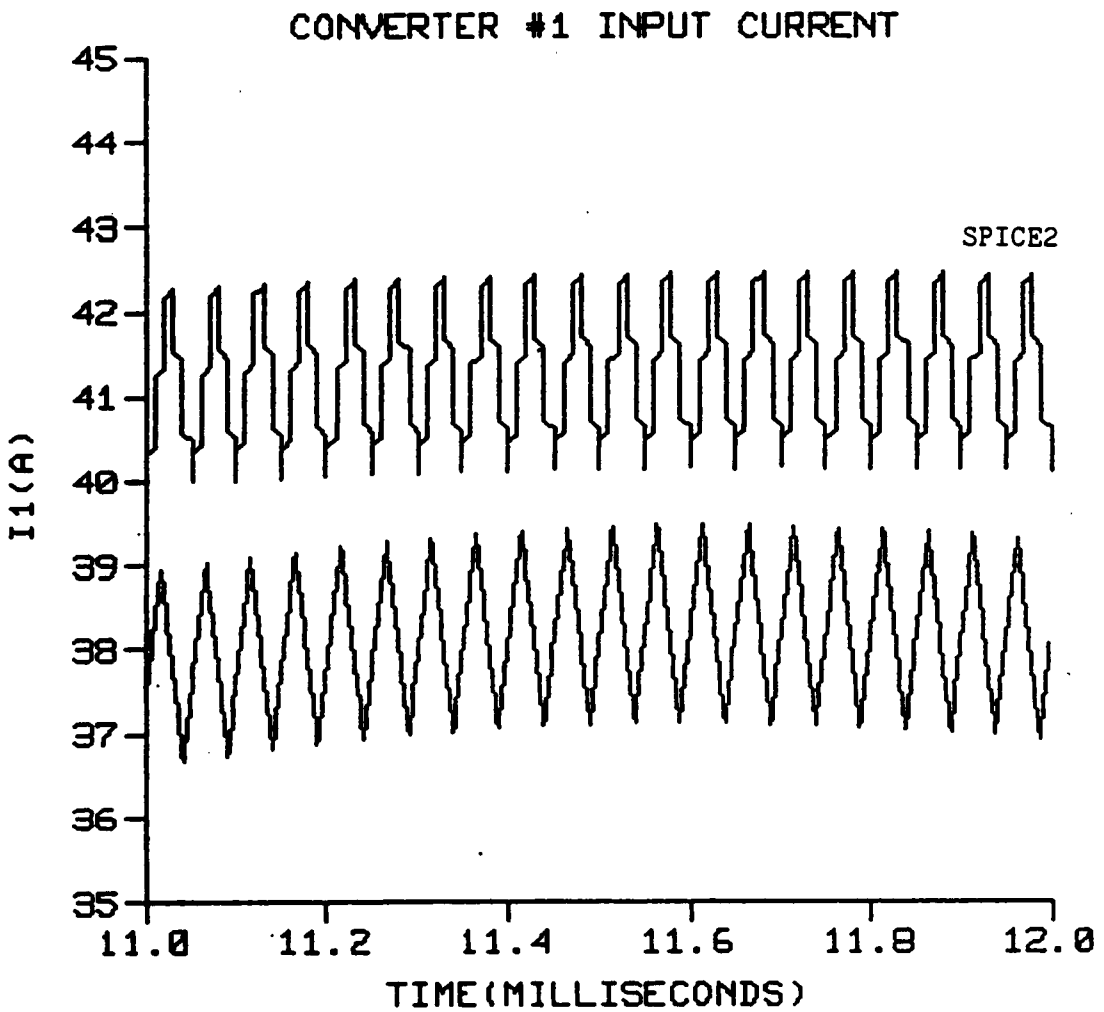

Figure 5.14. Converter #1 input current for 11 < t < 12 ms.

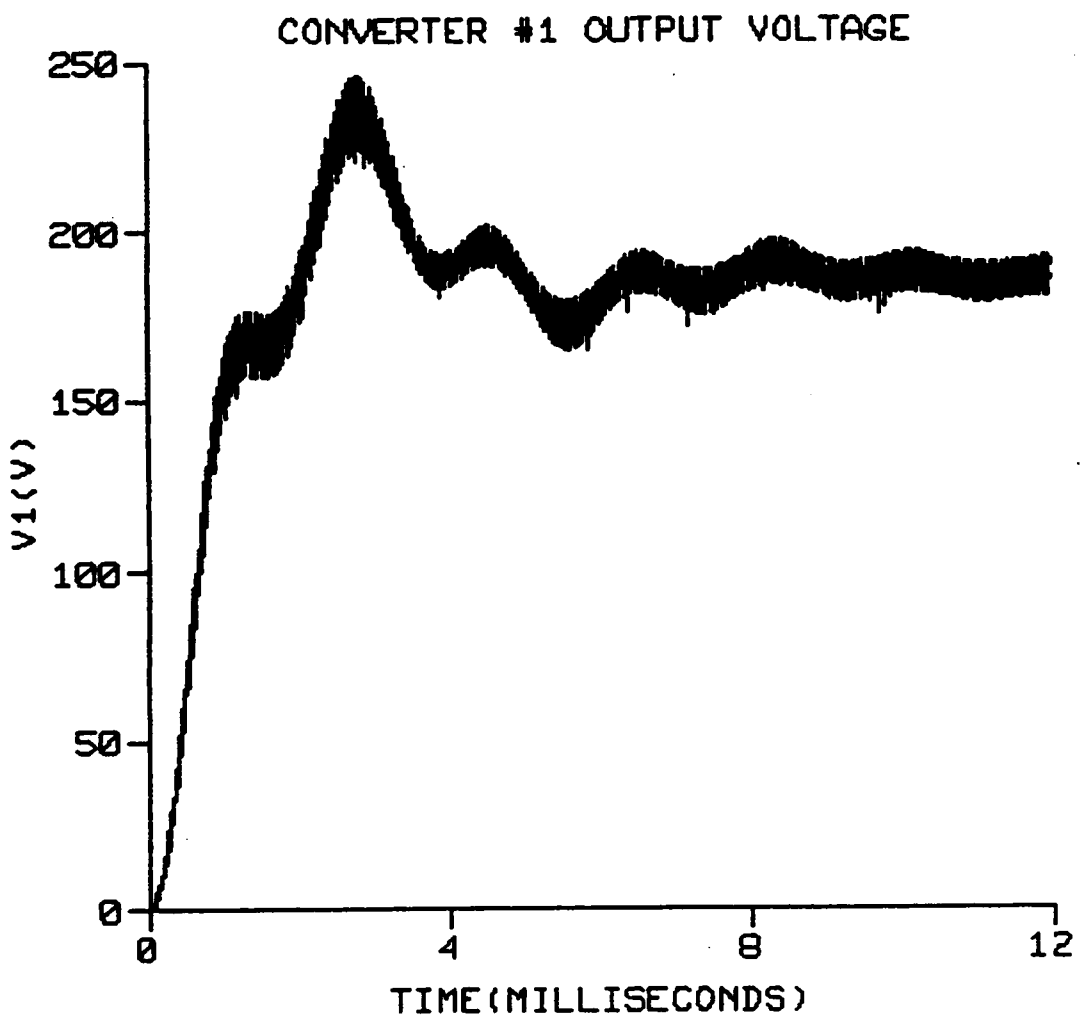

Figure 5.15. Converter #1 output voltage for $0 < t < 12$ ms.

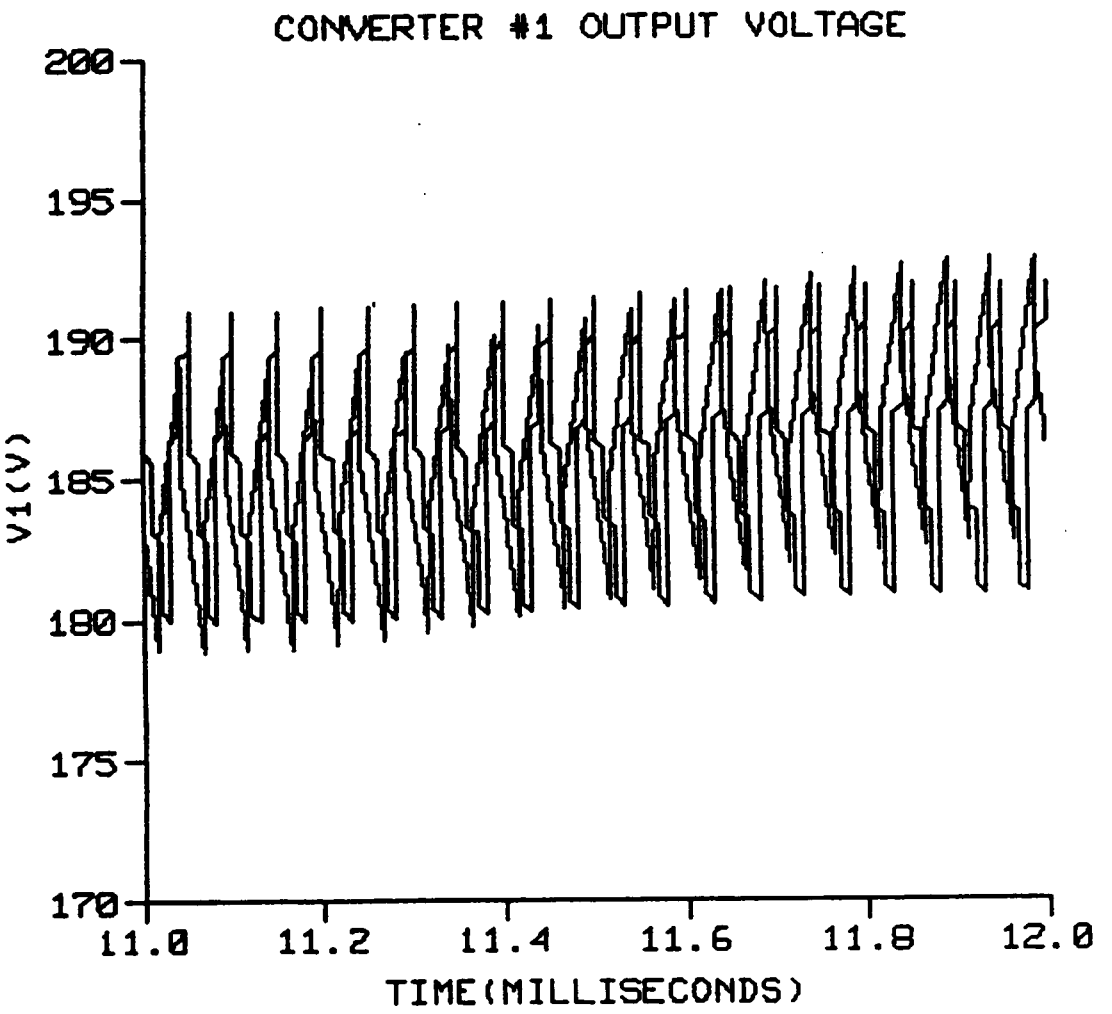

Figure 5.16. Converter #1 output voltage for 11 < t < 12 ms.

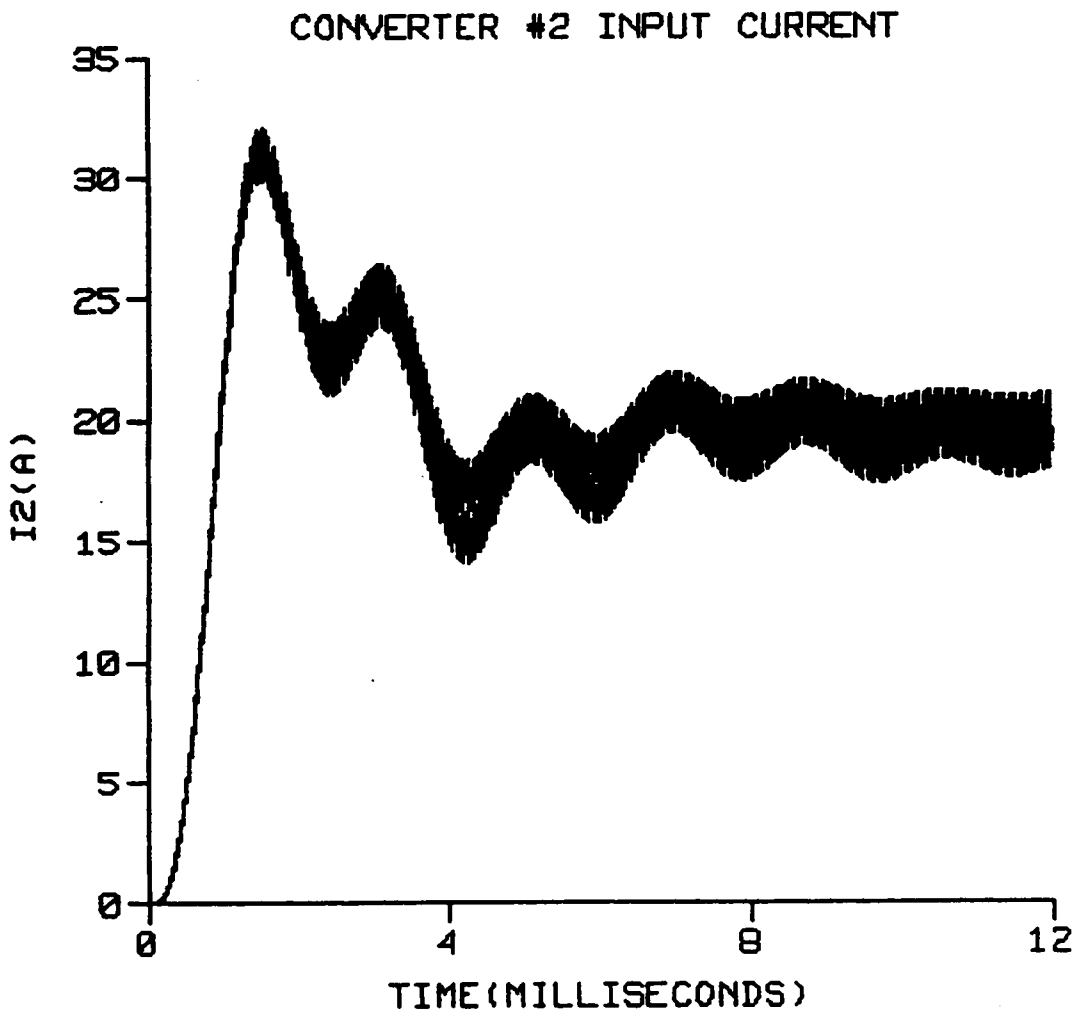

Figure 5.17. Converter #2 input current for $0 < t < 12$ ms.

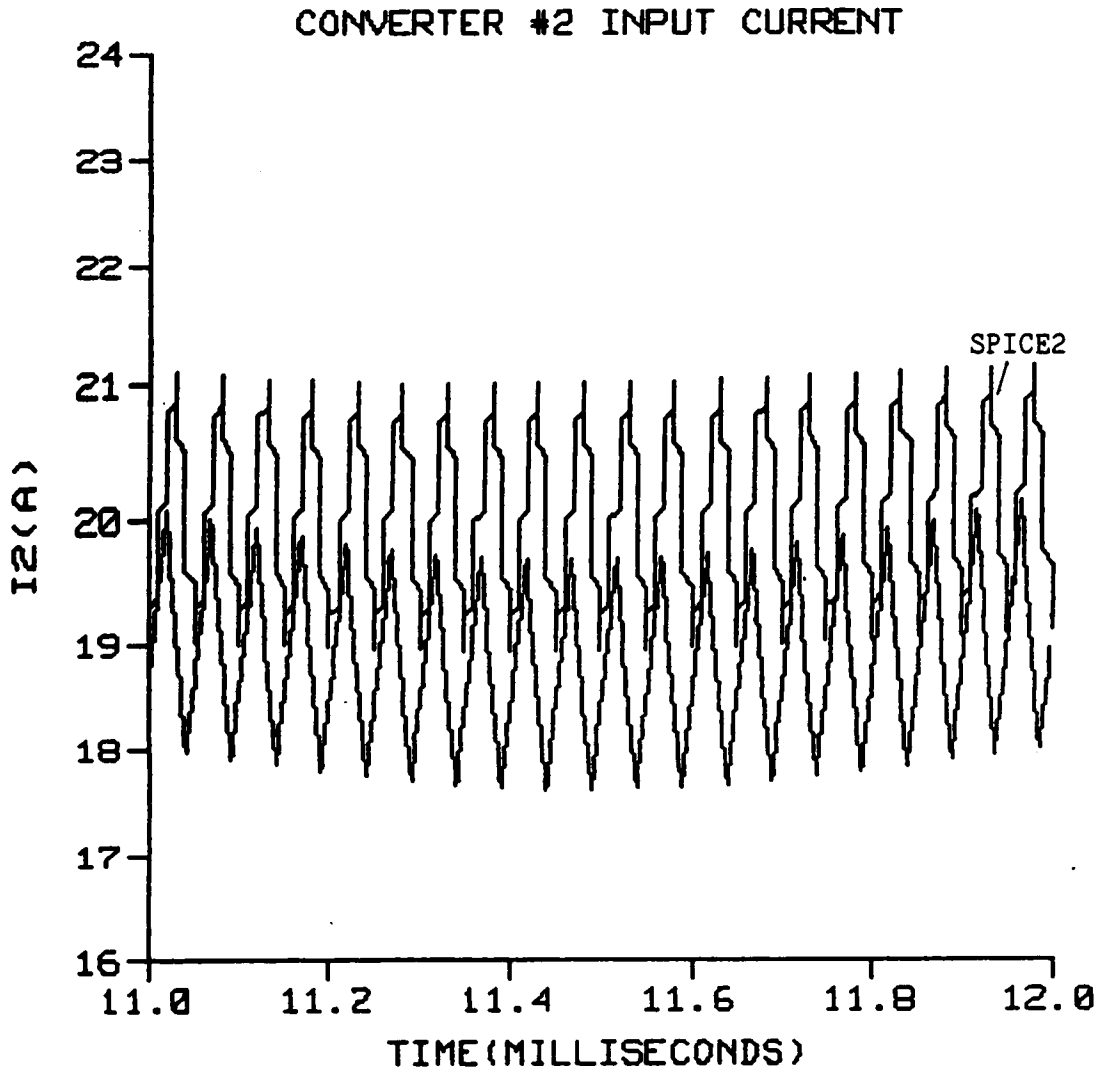

Figure 5.18. Converter #2 input current for 11 < t < 12 ms.

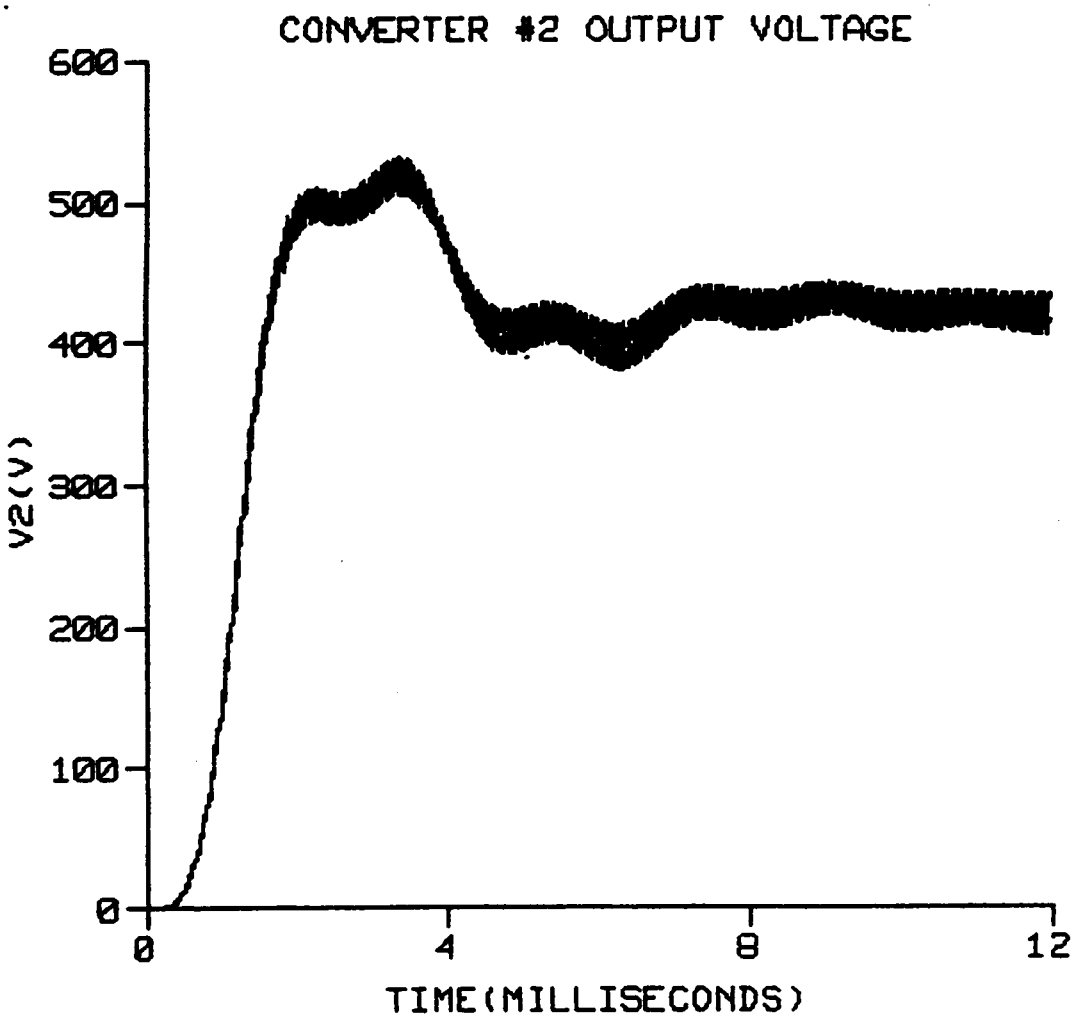

Figure 5.19. Converter #2 output voltage for $0 < t < 12$ ms.

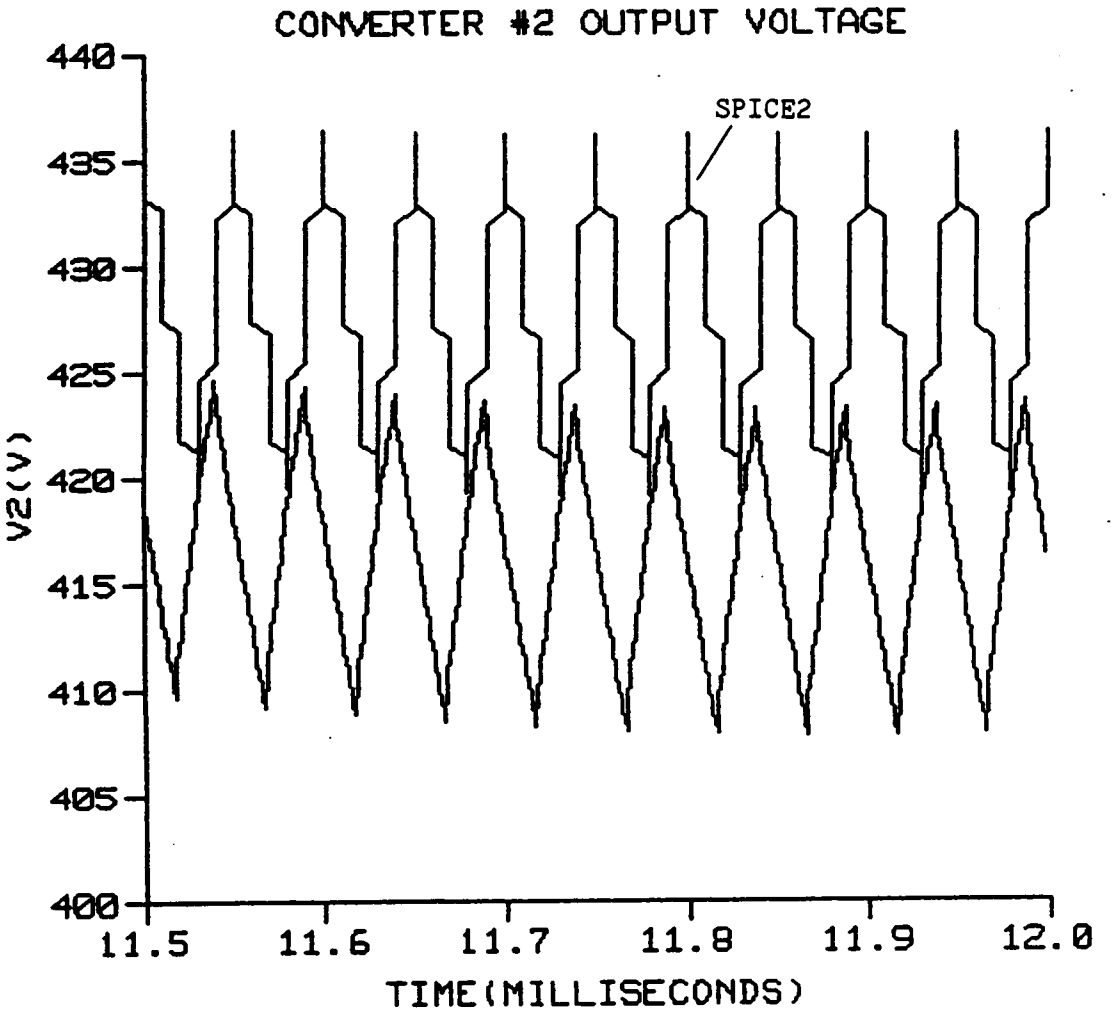

Figure 5.20. Converter #2 outut voltage for 11 < t < 12 ms.

5.4 Example System #3

This example presents some guidelines on the selection of the time step T. It consists of the resonant converter used in Example System #1 with a 10 Ω resistive load and a 100 V source. The switching frequency for this example is 20 kHz.

T must meet the following criteria: (1) the A and B matrices must be constant over the interval [0,T], (2) the inputs must not change appreciably over the interval [0,T], and (3) it must be selected so that entries in the state transition matrix do not vanish. If T is selected too large, all entries in the state transition matrix could be zero. The third requirement is related to the entries in the A matrix and is investigated in this example.

Recall that the A matrix for the parallel-loaded resonant converter is

$$A = \begin{bmatrix} -\frac{1}{L}\left\{ R_L + \frac{2R_{T1}R_{D1}R_{T3}R_{D3}}{\alpha_{13}} \right\} & 0 \\ 0 & -\frac{1}{R_C C} \end{bmatrix} \tag{5.8}$$

Approximate the a_{11} entry by $-R_L/L$. The state transition matrix for this case is

$$\Phi(t) = \begin{bmatrix} e^{-at} & 0 \\ 0 & e^{-bt} \end{bmatrix} \tag{5.9}$$

where $a = R_L/L$ and $b = 1/R_C C$. For this converter, $R_L = 0.1\ \Omega$, $L = 24\ \mu H$, $R_C = 0.1\ \Omega$, and $C = 1\ \mu F$. Substituting these values in (5.9) yields

$$\Phi(t) = \begin{bmatrix} e^{-4,166.7t} & 0 \\ 0 & e^{-10,000,000t} \end{bmatrix} \tag{5.10}$$

Examination of (5.10) shows that Φ_{22} approaches zero quickly as t increases. In fact, Φ_{22} equals 0.0000454 (e^{-10}) for $t = 1x10^{-6}$. Therefore, T must be selected so that Φ_{22} is not extremely small. For this example system, $1/a = 0.00024$ and $1/b = 1x10^{-7}$, so, as a guideline, T should be chosen at least one-tenth of the smaller value. This guideline is verified through simulation. The example system is simulated using the modular state variable approach for time steps of 10^{-6}, 10^{-7}, 10^{-8}, and 10^{-9} and the results compared with a SPICE2 simulation. In Figure 5.21, the converter output voltage predicted by the modular state variable approach with $T = 10^{-6}$ and SPICE2 are plotted. The modular state variable approach performs poorly for this value of T. Figure 5.22 shows that the modular state variable

performs better for $T = 10^{-7}$; however, it now predicts a higher peak value for the voltage. Figures 5.23 and 5.24 indicates that the modular state variable approach with $T = 10^{-8}$ or 10^{-9} calculates the same response as SPICE2. Therefore, a time step of 10^{-8}, which satisfies the guideline, must be used in the simulation.

Even though this example is not complex, it serves to illustrate how a maximum time step may be selected. The A matrix and the state transition matrix of a particular component are examined. A maximum time step can be selected based on this examination. Since the spacecraft power system is modeled as an interconnection of modular components, the A matrix of each component must be examined to determine the maximum time step. For the examples in this chapter, the maximum time step selected using this guideline has given results comparable to SPICE2. However, for large and complex systems, this guideline may select a time step too large. In this case, the selection of a time step can only be made through experience and experimentation.

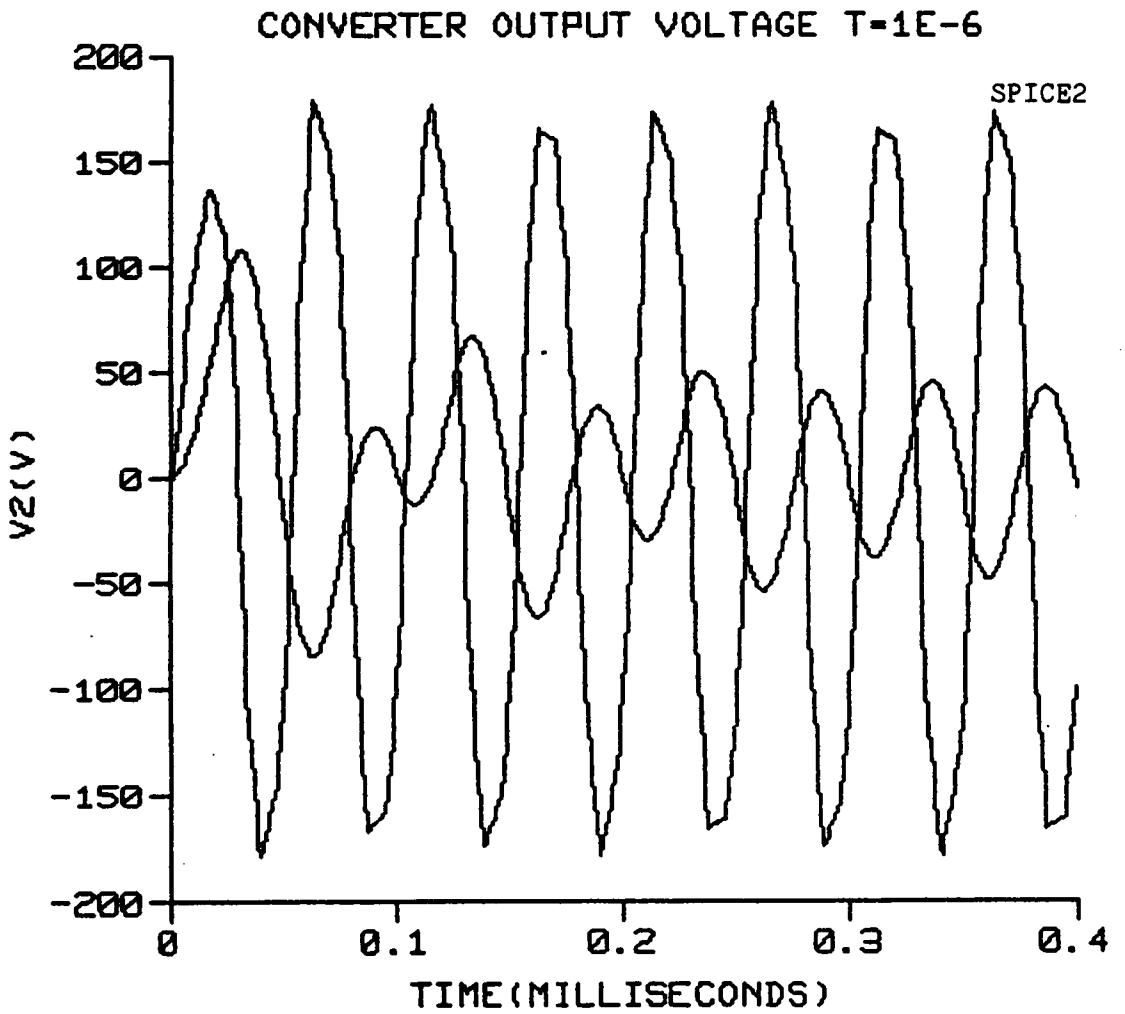

Figure 5.21. Converter output voltage for $T = 10^{-6}$.

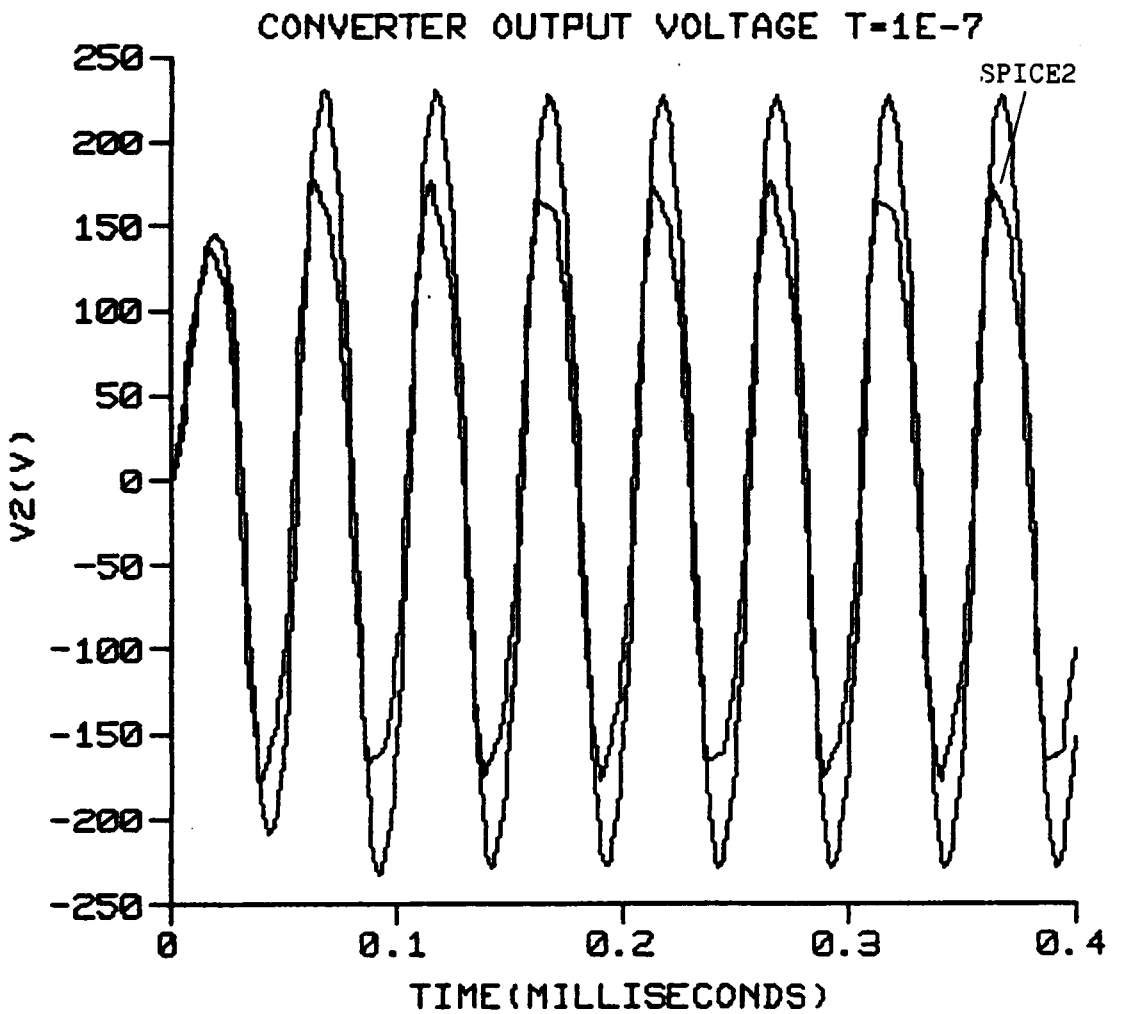

Figure 5.22. Converter output voltage for $T = 10^{-7}$.

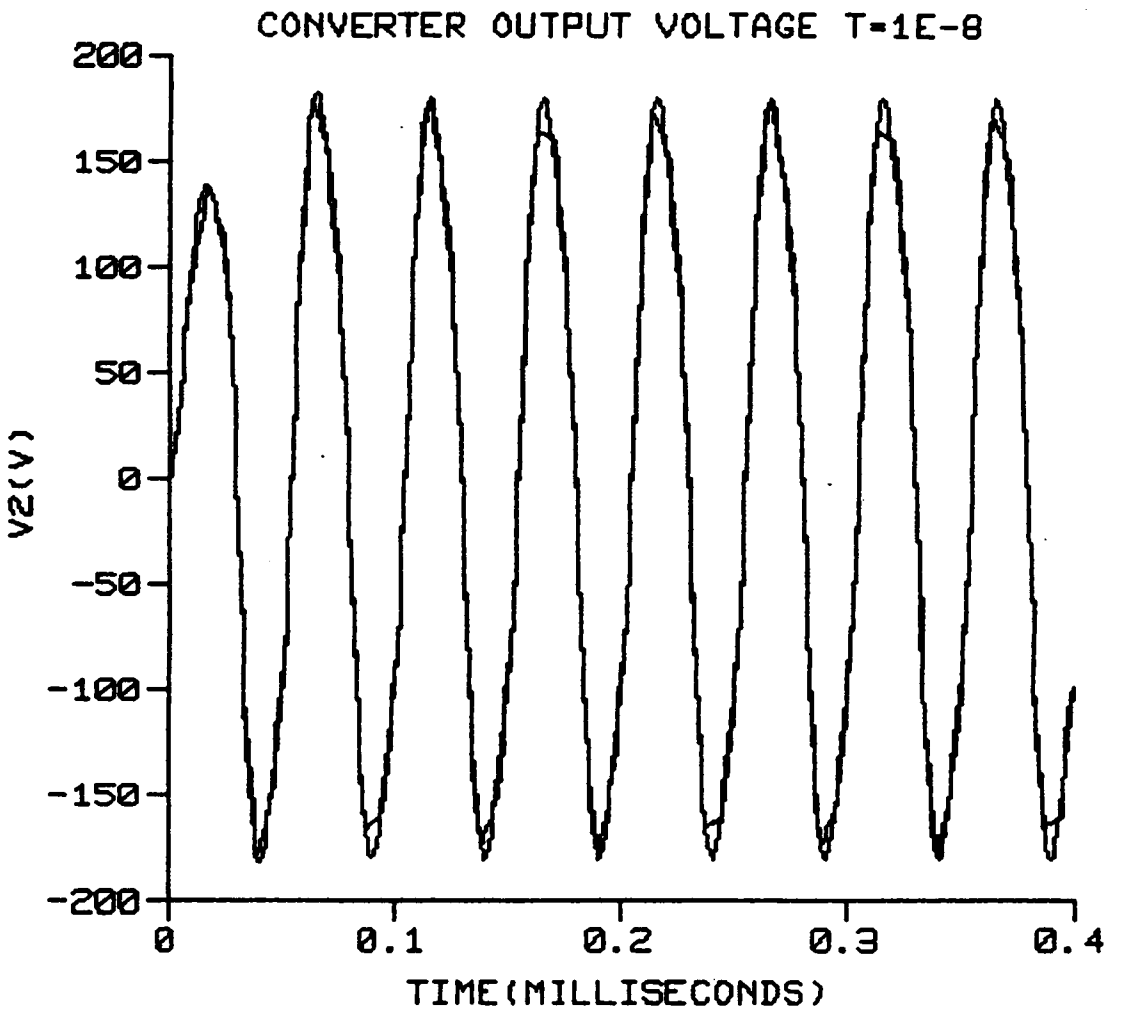

Figure 5.23. Converter output voltage for $T = 10^{-8}$.

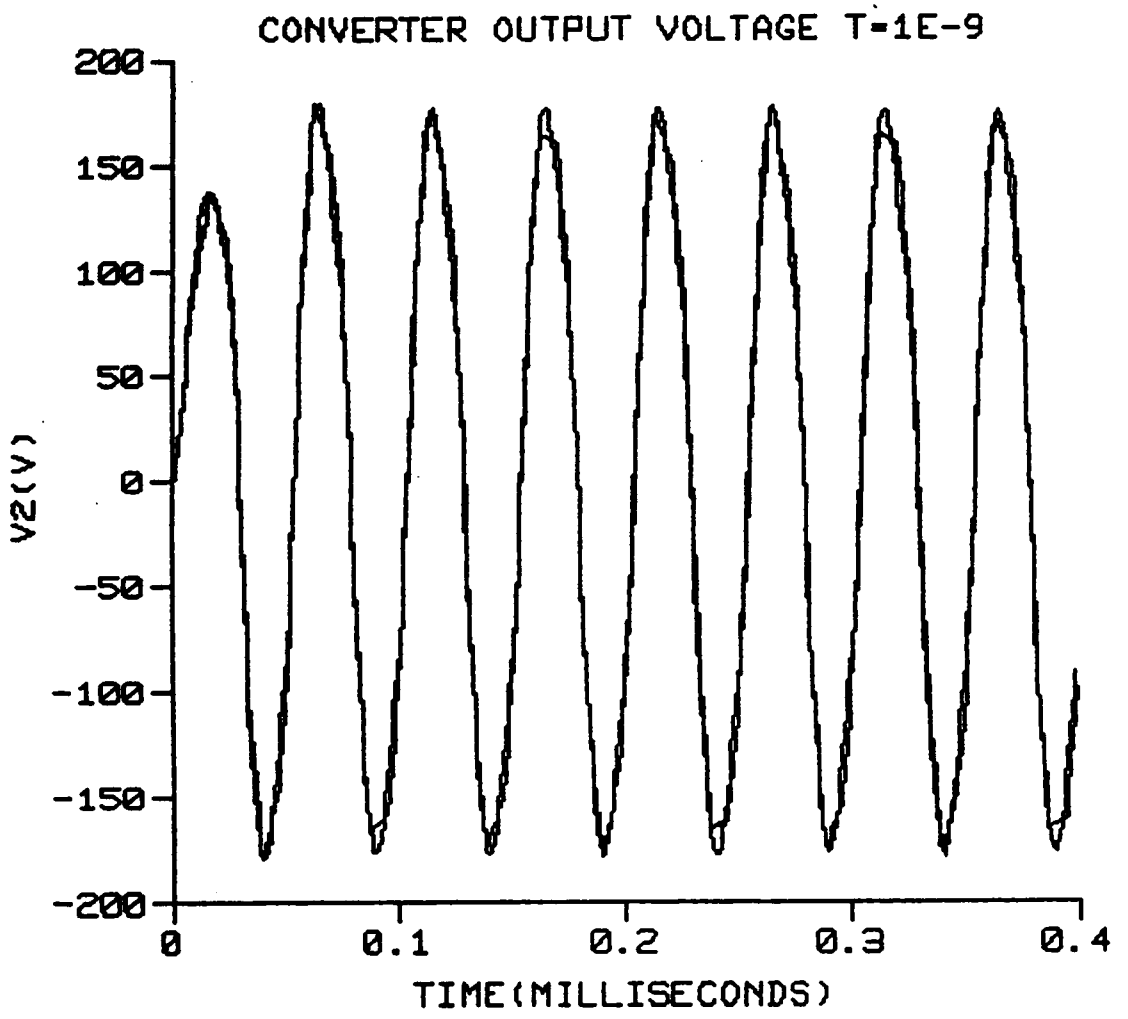

Figure 5.24. Converter output voltage for $T = 10^{-9}$.

CHAPTER 6. CONCLUSION

6.1 Summary

The spacecraft power systems of the future will be much larger and more complex than those of today because of increased power demands. Projected power levels are in the range of a few hundred kilowatts to a few megawatts. The digital computer must be utilized in the design and analysis of these future systems. A modular state variable approach has been proposed here as a tool in the design and analysis of such systems.

In the modular state variable approach, the spacecraft power system is considered as an interconnection of modular components. Each component is treated as a two-port network, and a state model is written with the port voltages as the inputs. An alternating solution procedure is employed in the simulation of the system. The state variables of each component are updated assuming that the inputs to that component are clamped for each time step. These computations proceed as if all components are decoupled. After all state variables have been updated, the inputs to all components are then calculated using network analysis principles.

The modular state variable approach has been compared to SPICE2 through the simulation of three test systems. The results of these simulations shows that the modular state variable approach and SPICE2

produce very nearly the same response. However, the modular state variable approach requires much less CPU time than SPICE2.

6.2 Suggestions for Further Work

DC-DC converters are controlled to limit the input current and to regulate the output voltage. Using pulse width modulation, these quantities are controlled by varying the duty ratio D. Various schemes for controlling these quantities should be investigated and modeled. Control functions could be considered as a separate component from the converter and treated as a multiport network. A state model could then be written in accord with the modular state variable approach.

This work has only considered the dynamic response of spacecraft power systems. The steady-state analysis of these systems is also of vital importance. Many of the analyses performed on terrestrial power systems are also applicable to spacecraft power systems. Since power converters will be an integral part of the spacecraft power system, a harmonic power flow will be needed. The control of spacecraft power systems should be investigated. Artificial intelligence techniques may be utilized in the control of the large and complex systems of the future. Load scheduling is a concern of the spacecraft power system engineer, whereas the utility power system engineer is concerned with generation scheduling.

REFERENCES

[1] Vincent C. Truscello and Herbert S. Davis, "Nuclear-electric power in space," IEEE Spectrum, December 1984, pp. 58-65.

[2] R.R. Barthelemy, L.D. Massie, and W.U. Borger, "Military Space Power Systems Technology for the Twenty-first Century," Proceedings of the 21st Intersociety Energy Conversion Engineering Conference, August 1986, Vol. 3, pp. 1401-1404.

[3] Donald L. Nored and Daniel T. Bernatowicz, "Electrical Power System Design for the U.S. Space Station," Proceedings of the 21st Intersociety Energy Conversion Engineering Conference, August 1986, Vol. 3, pp. 1416-1422.

[4] SPICE Version 2G - Users' Guide, Department of Electrical Engineering and Computer Science, University of California, Berkeley, CA.

[5] B.H. Cho and F.C. Lee, "Modeling and Analysis of Spacecraft Power Systems," IEEE Power Electronics Specialists Conference, 1985 Record, pp. 523-534.

[6] H.W. Dommel and N. Sato, "Fast Transient Stability Solutions," IEEE Transactions on Power Apparatus and Systems, Vol. PAS-91, No. 4, July/August 1972, pp. 1643-1650.

[7] S.B. Dewan and A. Straughen, Power Semiconductor Circuits, John Wiley and Sons, New York, 1975.

[8] R.D. Middlebrook and S. Cuk, Advances in Switched-Mode Power Conversion, Volume I, TESLAco, Pasadena, CA, 1983.

[9] R.D. Middlebrook and S. Cuk, Advances in Switched-Mode Power Conversion, Volume II, Pasadena, CA, 1983.

[10] R.D. Middlebrook and S. Cuk, Advances in Switched-Mode Power Conversion, Volume III, TESLAco, Pasadena, CA, 1983.

[11] John Cassinelli, "Analytical Modeling of Spacecraft Power Systems," NASA-CR-166820, April 1982.

[12] R.G. Hoft, Semiconductor Power Electronics, Van Nostrand Reinhold Company, New York, 1986.

[13] K. Kit Sum, Switch Mode Power Conversion: Basic Theory and Design, Marcel Dekker, Inc., New York, 1984.

[14] W.A. Blackwell and L.L. Grigsby, Introductory Network Theory, PWS Engineering, Boston, 1985.

[15] Irving G. Hansen and Gale R. Sundberg, "Space Station 20-kHz Power Management and Distribution System," IEEE Power Electronics Specialists Conference, 1986 Record, pp. 676-683.

[16] Francis C. Schwarz, "A Method of Resonant Current Pulse Modulation for Power Converters," IEEE Transactions on Industrial Electronics and Control Instrumentation, Vol. IECI-17, No. 3, May 1970, pp. 209-221.

[17] Francis C. Schwarz, "An Improved Method of Resonant Current Pulse Modulation for Power Converters," IEEE Transactions on Industrial Electronics and Control Instrumentation, Vol. IECI-23, No. 2, May 1976, pp. 133-141.

[18] Neville Mapham, "An SCR Inverter with Good Regulation and Sine-Wave Output," IEEE Transactions on Industry and General Applications, Vol. IGA-3, No. 2, March/April 1967, pp. 176-187.

[19] V. Vorperian and S. Cuk, "A Complete DC Analysis of the Series Resonant Converter," IEEE Power Electronics Specialists Conference, 1982 Record, pp. 85-100.

[20] V. Vorperian and S. Cuk, "Small Signal Analysis of Resonant Converters," IEEE Power Electronics Specialists Conference, 1983 Record, pp. 269-282.

[21] R. King and T.A. Stuart, "A Normalized Model for the Half-Bridge Series Resonant Converter," IEEE Transactions on Aerospace and Electronic Systems, Vol. AES-17, No. 2, March 1981, pp. 190-198.

[22] R.J. King and T.A. Stuart, "Modeling the Full-Bridge Series-Resonant Power Converter," IEEE Transactions on Aerospace and Electronic Systems, Vol. AES-18, No. 4, July 1982, pp. 449-459.

[23] A.S. Kislovski, "A Contribution to Steady-State Modeling of Half-Bridge Series-Resonant Power Cells," IEEE Transactions on Power Electronics, Vol. PE-1, No. 3, July 1986, pp. 161-166.

[24] S.D. Johnson and R.W. Erickson, "Steady-State Analysis and Design of the Parallel Resonant Converter," IEEE Power Electronics Specialists Conference, 1986 Record, pp. 154-165.

[25] A. Witulski and R.W. Erickson, "Steady-State Analysis of the Series Resonant Converter," IEEE Transactions on Aerospace and Electronic Systems, Vol. AES-21, No. 6, November 1985, pp. 791-799.

[26] R. Oruganti and F.C. Lee, "State-Plane Analysis of Parallel Resonant Converter," IEEE Power Electronics Specialists Conference, 1986 Record, pp. 56-73.

[27] C.Q. Lee and K. Siri, "Analysis and Design of Series Resonant Converter by State-Plane Diagram," IEEE Transactions on Aerospace and Electronic Systems, Vol. AES-22, No. 6, November 1986, pp. 757-763.

[28] R.J. King and T.A. Stuart, "A Large-Signal Dynamic Simulation for the Series Resonant Converter," IEEE Transactions on Aerospace and Electronic Systems, Vol. AES-19, No. 6, November 1983, pp. 859-870.

[29] S.S. Kelkar and Fred C.Y. Lee, "A Fast Time Domain Digital Simulation Technique for Power Converters: Application to a Buck Converter with Feedforward Compensation," IEEE Transactions on Power Electronics, Vol. PE-1, No. 1, January 1986, pp. 21-31.

[30] Paul M. DeRusso, Rob J. Roy, and Charles M. Close, State Variables for Engineers, John Wiley and Sons, New York, 1965.

[31] J. Mildice and L. Wappes, "Resonant ac power system proof-of-concept," NASA CR-175069, 1986.

[32] B.W. Williams, Power Electronics: Device, Drivers and Applications, John Wiley and Sons, New York, 1987.

[33] R.D. Middlebrook and Slobodan Cuk, "A General Unified Approach to Modelling Switching-Converter Power Stages," IEEE Power Electronics Specialists Conference, 1976 Record, pp. 18-34.

[34] S. Cuk and R.D. Middlebrook, "A General Unified Approach to Modelling Switching DC-to-DC Converters in Discontinuous Conduction Mode," IEEE Power Electronics Specialists Conference, 1977 Record, pp. 36-57.

[35] W.M. Polivka, P.R.K. Chetty, and R.D. Middlebrook, "State-Space Average Modelling of Converters with Parasitics and Storage-Time Modulation," IEEE Power Electronics Specialists Conference, 1980 Record, pp. 119-143.

[36] R.C. Wong, G.E. Rodriguez, H.A. Owen, Jr., and T.G. Wilson, "Application of Small-Signal Modeling and Measurement Techniques to the Stability Analysis of an Integrated Switching-Mode Power System," IEEE Power Electronics Specialists Conference, 1980 Record, pp. 104-118.

[37] G.W. Wester and R.D. Middlebrook, "Low Frequency Characterization of Switched DC-to-DC Converters," IEEE Power Electronics Specialists Conference, 1972 Record, pp. 9-20.

[38] F.C. Lee, Y. Yu, and J.E. Triner, "Modeling of Switching Regulator Power Stages With and Without Zero-Inductor-Current Dwell Time," IEEE Power Electronics Specialists Conference, 1976 Record, pp. 62-72.

[39] F.C. Lee, R.P. Iwens, Y. Yu, and J.E. Triner, "Generalized Computer-Aided Discrete Time Domain Modeling and Analysis of DC-DC Converters," IEEE Power Electronics Specialists Conference, 1977 Record, pp. 58-69.

[40] Arthur R. Brown and R.D. Middlebrook, "Sampled-Data Modeling of Switching Regulators," IEEE Power Electronics Specialists Conference, 1981 Record, pp. 349-369.

[41] D.J. Shortt and F.C. Lee, "An Improved Switching Converter Model Using Discrete and Average Techniques," IEEE Power Electronics Specialists Conference, 1982 Record, pp. 199-212.

[42] D.J. Shortt and F.C. Lee, "Extensions of the Discrete-Average Models for Converter Power Stages," IEEE Power Electronics Specialists Conference, 1983 Record, pp. 23-27.

[43] R.P. Iwens, Y. Yu, and J.E. Triner, "Time Domain Modelling and Stability Analysis of an Integral Pulse Frequency Modulated DC to DC Power Converter," IEEE Power Electronics Specialists Conference, 1975 Record, pp. 75-90.

[44] R.W. Erickson, S. Cuk, and R.D. Middlebrook, "Large-Signal Modelling and Analysis of Switching Regulators," IEEE Power Electronics Specialists Conference, 1982 Record, pp. 240-250.

[45] R.C. Wong, H.A. Owen, Jr., and T.G. Wilson, "A Fast Algorithm for the Time-Domain Simulation of Switched-Mode Piecewise-Linear Systems," IEEE Power Electronics Specialists Conference, 1984 Record, pp. 281-296.

[46] H.A. Owen, A. Capel, and J.G. Ferrante, "Simulation and Analysis Methods for Sampled Power Electronic Systems," IEEE Power Electronics Specialists Conference, 1976 Record, pp. 45-55.

[47] R.D. Middlebrook and S. Cuk, "Modelling and Analysis Methods for DC-to-DC Switching Converters," IEEE International Semiconductor Power Converter Conference, 1977 Record, pp. 90-111.

[48] R.J. King and T.A. Stuart, "Inherent Overload Protection for the Series Resonant Converter," IEEE Transactions on Aerospace and Electronic Systems, Vol. AES-19, No. 6, November 1983, pp. 820-830.

[49] R.J. King and T.A. Stuart, "Transformer Induced Instability of the Series Resonant Converter," IEEE Transactions on Aerospace and Electronic Systems, Vol. AES-19, No. 3, May 1983, pp. 474-482.

[50] C.T. Chen, Introduction to Linear System Theory, Holt, Rinehart and Winston, Inc., New York, 1970.

[51] William L. Brogan, Modern Control Theory, Prentice-Hall, Inc., Englewood Cliffs, New Jersey, 1985.

The vita has been removed from the scanned document